SLOW FLOW OF A BINGHAM FLUID IN A GAP OF SLOWLY VARYING WIDTH

by

DANIEL PADRAIGH RYAN

B.Sc. (Mathematics) University of Minnesota, 2000

A THESIS SUBMITTED IN PARTIAL FULFILLMENT OF

THE REQUIREMENTS FOR THE DEGREE OF

MASTER OF SCIENCE

in

THE FACULTY OF GRADUATE STUDIES

Institute of Applied Mathematics, Department of Mathematics

We accept this thesis as conforming
to the required standard

.....

.....

.....

.....

THE UNIVERSITY OF BRITISH COLUMBIA

September 2003

In presenting this thesis in partial fulfillment of the requirements for an advanced degree at the University of British Columbia, I agree that the Library shall make it freely available for reference and study. I further agree that permission for extensive copying of this thesis for scholarly purposes may be granted by the head of my department or by his or her representatives. It is understood that copying or publication of this thesis for financial gain shall not be allowed without my written permission.

(Signature) _____

Department of Mathematics
The University of British Columbia
Vancouver, Canada

Date _____

Abstract

The slow Poiseuille flow of a Bingham fluid in an infinitely long gap of slowly varying width is considered. A consistent analytical theory is developed using a lubrication scaling without deviating from the Bingham model. It is shown that for sufficiently small gap width variations there is a rigid plug zone around the center of the gap. A numerical treatment of the problem is also presented using the method of augmented Lagrangian.

Table of Contents

List of Tables

List of Figures

Acknowledgement

This research was conducted under the supervision of Dr. Ian Frigaard. I would like to thank him for for his guidance, advice, encouragement, and extreme patience throughout.

I would also like to thank NSERC and Schlumberger Cambridge Research for funding the research in this thesis, via collaborative research grant CRD 245434. The Pacific Institute for Mathematical Sciences is also thanked for their additional funding.

Chapter 1
Introduction

A Bingham fluid is an incompressible visco-plastic yield stress fluid. It is characterized by the fact that when the stress is below the yield stress, the rate-of-strain is zero, and the fluid moves as a rigid solid. When the stress is above this yield value, the rate-of-strain is in a linear relationship with the stress and the fluid flows in a viscous manner.

Here, we consider the 2-D Poiseuille flow of a Bingham fluid in a gap of slowly varying width. The gap is assumed to be symmetric about the centerline and to have periodic width in the flow direction. This results in a flow with zero shear stress on the centerline. As a result, if the variation of the gap width is kept small enough, the stress on the centerline will be below the yield value, and a solid plug will exist along the infinite length of the gap. According to the Bingham model, this solid plug will move with uniform speed. See Fig. 1.1 for a sketch of the flow and domain.

It is known that when a lubrication scaling is used with a Bingham fluid, there is an inconsistency at leading order. This inconsistency is that the lubrication model shows a plug existing, yet shows a non-uniform speed for the plug. This is not allowed by the Bingham model which requires the plug to behave like a rigid solid. In some instances people have shown that this is because there is not actually a plug region because the stress is, in fact, slightly above the yield value. Others have proposed alternate constitutive models for the fluid in order to resolve this inconsistency. Some such models use methods of viscosity regularization in which the solid is replaced by a fluid of large viscosity (e.g. [9] & [10]) and the visco-elastic model in which the rigid solid is replaced with an elastic.

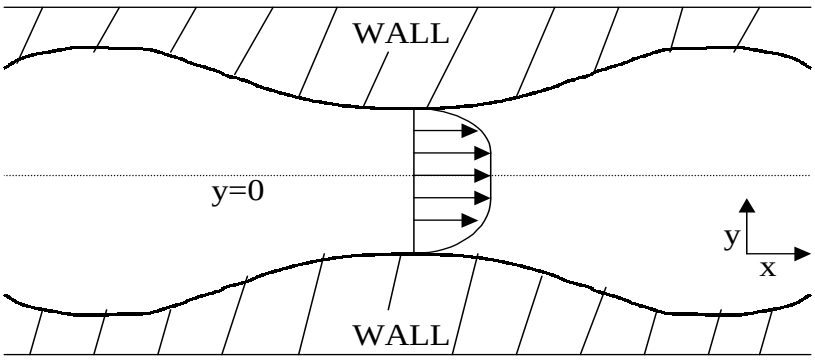

Figure 1.1: A sketch of the 2-D flow that will be examined.

In this problem, we know that when the gap width variation is kept small enough there must be a rigid plug along the length of the gap. Herein, we will use a lubrication scaling, and then resolve the plug inconsistency without straying from the Bingham model. This will be done by constructing first and second order corrections to the pressure and velocity fields, resulting in an asymptotic solution that describes a rigid plug with uniform speed. Note that throughout this analysis, the words ”gap” and ”channel” are used interchangeably.

An analytical technique for determining the uniform speed of the plug will also be developed at the end of Chapter 5. It will use an extremum principle for the solution stress field to determine the appropriate plug velocity. A criteria for determining when the gap width variation is large enough to break the plug will also be presented in Chapter 6.

A finite element formulation of the problem will be derived and implemented in Chapters 3 and 4. It will use the method of augmented Lagrangian, which allows accurate computation of the unyielded plug region, wherein, the rate-of-strain will be computed to be zero.

The agreement between the results of the numeric and analytic approaches will be discussed in Chapters 5 and 6.

Chapter 2
Equations and Scalings

2.1 Dimensional Equations

We start with the following equations for the flow of an incompressible Bingham fluid through a 2-D gap.

The flow is modelled by the Navier-Stokes Equations coupled with the Bingham fluid constitutive laws.

2.1.1 The Equations of Motion

These equations relate the velocity $\mathbf{u} = \langle \hat{u}\ ,\ \hat{v} \rangle$, pressure $\hat{p}$ and the deviatoric stress-tensor $\hat{\tau}_{ij}$. The fluid is assumed to have constant density $\hat{\rho}$, and to be incompressible, and is governed by

$$\hat{\rho}(\frac{\partial \hat{u}}{\partial \hat{t}} + \hat{u}\frac{\partial \hat{u}}{\partial \hat{x}} + \hat{v}\frac{\partial \hat{u}}{\partial \hat{y}}) = -\frac{\partial \hat{p}}{\partial \hat{x}} + \frac{\partial}{\partial \hat{x}}\hat{\tau}_{xx} + \frac{\partial}{\partial \hat{y}}\hat{\tau}_{xy}, \tag{2.1}$$

$$\hat{\rho}(\frac{\partial \hat{v}}{\partial \hat{t}} + \hat{u}\frac{\partial \hat{v}}{\partial \hat{x}} + \hat{v}\frac{\partial \hat{v}}{\partial \hat{y}}) = -\frac{\partial \hat{p}}{\partial \hat{y}} + \frac{\partial}{\partial \hat{x}}\hat{\tau}_{xy} + \frac{\partial}{\partial \hat{y}}\hat{\tau}_{yy}, \tag{2.2}$$

$$\frac{\partial \hat{u}}{\partial \hat{x}} + \frac{\partial \hat{v}}{\partial \hat{y}} = 0. \tag{2.3}$$

The rate-of-strain tensor,$\hat{\dot{\gamma}}_{ij}$, and its second invariant, $\hat{\dot{\gamma}}$, are defined as

$$\hat{\dot{\gamma}}_{xy} = \frac{\partial \hat{u}}{\partial \hat{y}} + \frac{\partial \hat{v}}{\partial \hat{x}}, \tag{2.4}$$

$$\hat{\dot{\gamma}}_{xx} = 2\frac{\partial \hat{u}}{\partial \hat{x}}, \tag{2.5}$$

$$\hat{\dot{\gamma}}_{yy} = 2\frac{\partial \hat{v}}{\partial \hat{y}}, \tag{2.6}$$

$$\hat{\dot{\gamma}} = (\sum_{i,j=1}^{2} \frac{1}{2}\hat{\dot{\gamma}}_{ij}^2)^{\frac{1}{2}}. \tag{2.7}$$

Let $\hat{\tau}_y$ be the yield stress of the fluid, $\hat{\mu}$ be the plastic viscosity, $\hat{\tau}_{ij}$ be the deviatoric stress tensor, and $\hat{\tau}$ be the second invariant of $\hat{\tau}_{ij}$, i.e. the stress. The Bingham fluid constitutive laws are

$$\begin{aligned} \hat{\tau}_{ij} = (\hat{\mu} + \frac{\hat{\tau}_y}{\hat{\dot{\gamma}}})\hat{\dot{\gamma}}_{ij} \iff \quad & \hat{\tau} > \hat{\tau}_y, \\ \hat{\dot{\gamma}} = 0 \iff \quad & \hat{\tau} \leq \hat{\tau}_y, \end{aligned} \tag{2.8}$$

where

$$\hat{\tau} = (\sum_{i,j=1}^{2} \frac{1}{2}\hat{\tau}_{ij}^2)^{\frac{1}{2}}. \tag{2.9}$$

It should be noted that it is not possible to explicitly express the deviatoric stress in terms of the rate-of-strain when in a region where the stress is below the yield value, $\hat{\tau}_y$.

The areas where $\hat{\tau} < \hat{\tau}_y$ have a zero rate-of-strain, hence they move like a rigid solid, and will be hereinafter referred to as "plug regions".

2.1.2 Domain and Constraints

Fig. 2.1 is a sketch of the domain. In order to simplify the problem, it is assumed that the gap walls are symmetric about the centerline, $\hat{y} = 0$. It is also assumed that the gap walls are periodic in the $\hat{x}$ spatial dimension with periodicity $\hat{L}$. Because of the symmetry about $\hat{y} = 0$, we can restrict our attention to only positive $\hat{y}$.

We will assume that there is a fixed average flow rate, $\hat{U}_0$, being pumped into the gap infinitely downstream. This can be expressed using the mean flow rate $\hat{U}_0$ and mean half-gap width $\hat{D}$ as

$$\int_0^{\hat{y}_i(\hat{x})} \hat{u}\, d\hat{y} = \hat{U}_0\hat{D} \quad \forall \hat{x}, \tag{2.10}$$

where $\hat{y}_i(\hat{x})$ is the local half-width of the slot.

There is a no-slip condition on the velocity field at $\pm\hat{y}_i(\hat{x})$, the channel walls. This means

$$\hat{u} = \hat{v} = 0 \ \text{ on } \ \hat{y} = \hat{y}_i(\hat{x}). \tag{2.11}$$

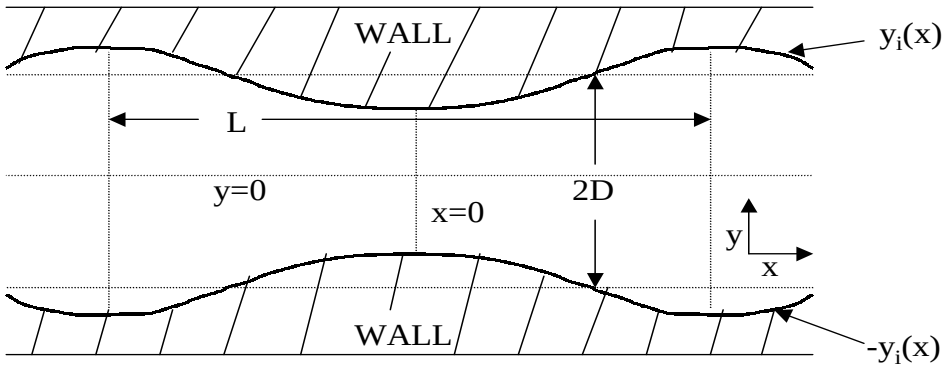

Figure 2.1: A sketch of the domain before scaling.

As a result of the symmetry of the flow about $\hat{y} = 0$, we know there is no shear stress on the centerline, i.e.

$$\hat{\tau}_{xy} = 0 \ \text{ on } \ \hat{y} = 0. \tag{2.12}$$

2.2 Non-Dimensionalization

We now use the mean half-gap width, $\hat{D}$, to scale the space variables, and the mean flow rate, $\hat{U}_0$, to scale the velocity components.

$$\begin{aligned}
\hat{x} &= \hat{D}x & \hat{y} &= \hat{D}y \\
\hat{u} &= \hat{U}_0 u & \hat{v} &= \hat{U}_0 v \\
\hat{t} &= \frac{\hat{D}}{\hat{U}_0} t & \hat{p} &= \frac{\hat{\mu}\hat{U}_0}{\hat{D}} p \\
\hat{\dot{\gamma}}_{xy} &= \frac{\hat{U}_0}{\hat{D}} \dot{\gamma}_{xy} & \hat{\tau}_{xy} &= \frac{\hat{\mu}\hat{U}_0}{\hat{D}} \tau_{xy} \\
\hat{\dot{\gamma}}_{yx} &= \frac{\hat{U}_0}{\hat{D}} \dot{\gamma}_{yx} & \hat{\tau}_{yx} &= \frac{\hat{\mu}\hat{U}_0}{\hat{D}} \tau_{yx} \\
\hat{\dot{\gamma}}_{xx} &= \frac{\hat{U}_0}{\hat{D}} \dot{\gamma}_{xx} & \hat{\tau}_{xx} &= \frac{\hat{\mu}\hat{U}_0}{\hat{D}} \tau_{xx} \\
\hat{\dot{\gamma}}_{yy} &= \frac{\hat{U}_0}{\hat{D}} \dot{\gamma}_{yy} & \hat{\tau}_{yy} &= \frac{\hat{\mu}\hat{U}_0}{\hat{D}} \tau_{yy} \\
\hat{\dot{\gamma}} &= \frac{\hat{U}_0}{\hat{D}} \dot{\gamma} & \hat{\tau} &= \frac{\hat{\mu}\hat{U}_0}{\hat{D}} \tau
\end{aligned} \tag{2.13}$$

Substituting these non-dimensional variables into the momentum equations yield

$$Re(\frac{\partial u}{\partial t} + u\frac{\partial u}{\partial x} + v\frac{\partial u}{\partial y}) = -\frac{\partial p}{\partial x} + \frac{\partial}{\partial x}\tau_{xx} + \frac{\partial}{\partial y}\tau_{xy} \tag{2.14}$$

$$Re(\frac{\partial v}{\partial t} + u\frac{\partial v}{\partial x} + v\frac{\partial v}{\partial y}) = -\frac{\partial p}{\partial y} + \frac{\partial}{\partial x}\tau_{xy} + \frac{\partial}{\partial y}\tau_{yy} \tag{2.15}$$

$$\frac{\partial u}{\partial x} + \frac{\partial v}{\partial y} = 0. \tag{2.16}$$

In (2.14) and (2.15), Re is the Reynold's number, a dimensionless quantity measuring the ratio of inertial effects to viscous effects which is given by

$$Re \equiv \frac{\hat{\rho}\hat{U}_0\hat{D}}{\hat{\mu}}. \tag{2.17}$$

The non-dimensional rate-of-strain tensor is now,

$$\dot{\gamma}_{xy} = \frac{\partial u}{\partial y} + \frac{\partial v}{\partial x}, \tag{2.18}$$

$$\dot{\gamma}_{xx} = 2\frac{\partial u}{\partial x}, \tag{2.19}$$

$$\dot{\gamma}_{yy} = 2\frac{\partial v}{\partial y}. \tag{2.20}$$

By introducing Bingham number,B, our constitutive relations become

$$\tau_{ij} = (1 + \frac{B}{\dot{\gamma}})\dot{\gamma}_{ij} \iff \quad \tau > B \tag{2.21}$$

$$\dot{\gamma} = 0 \iff \quad \tau \leq B.$$

The Bingham number is a dimensionless parameter that represents a ratio between the yield strength of the fluid and the size of the viscous terms, and is given by

$$B \equiv \frac{\hat{\tau}_y\hat{D}}{\hat{\mu}\hat{U}_0}. \tag{2.22}$$

The condition of incompressibility gives $\dot{\gamma}_{xx} = -\dot{\gamma}_{yy}$, which in turn gives $\tau_{xx} = -\tau_{yy}$. This allows us to write the second invariants of the rate-of-strain tensor and the deviatoric stress tensor as

$$\dot{\gamma} = (\dot{\gamma}_{xy}^2 + \dot{\gamma}_{xx}^2)^{\frac{1}{2}}, \tag{2.23}$$

and

$$\tau = (\tau_{xy}^2 + \tau_{xx}^2)^{\frac{1}{2}}. \tag{2.24}$$

2.3 The Lubrication Approximation

The approach is numerical in Chapters 3 and 4. Afterwards, we use a lubrication approximation which we derive below to study the flow analytically.

For analytical purposes, we make use of the fact that the gap has a slowly varying width along the length of the channel, so the characteristic length, $\hat{L}$, is much larger than the mean half-width, $\hat{D}$. Taking this into account, we choose to scale $\hat{x}$ and $\hat{y}$ differently for the analytic approach. This type of scaling is referred to as a lubrication scaling.

$$\begin{aligned}
\hat{x} &= \hat{L}x & \hat{y} &= \hat{D}y \\
\hat{u} &= \hat{U}_0 u & \hat{v} &= \frac{\hat{D}\hat{U}_0}{\hat{L}}v \\
\hat{t} &= \frac{\hat{L}}{\hat{U}_0}t & \hat{p} &= \frac{\hat{\mu}\hat{U}_0\hat{L}}{\hat{D}^2}p \\
\hat{\dot{\gamma}}_{xy} &= \frac{\hat{U}_0}{\hat{D}}\dot{\gamma}_{xy} & \hat{\tau}_{xy} &= \frac{\hat{\mu}\hat{U}_0}{\hat{D}}\tau_{xy} \\
\hat{\dot{\gamma}}_{yx} &= \frac{\hat{U}_0}{\hat{D}}\dot{\gamma}_{yx} & \hat{\tau}_{yx} &= \frac{\hat{\mu}\hat{U}_0}{\hat{D}}\tau_{yx} \\
\hat{\dot{\gamma}}_{xx} &= \frac{\hat{U}_0}{\hat{L}}\dot{\gamma}_{xx} & \hat{\tau}_{xx} &= \frac{\hat{\mu}\hat{U}_0}{\hat{L}}\tau_{xx} \\
\hat{\dot{\gamma}}_{yy} &= \frac{\hat{U}_0}{\hat{L}}\dot{\gamma}_{yy} & \hat{\tau}_{yy} &= \frac{\hat{\mu}\hat{U}_0}{\hat{L}}\tau_{yy} \\
\hat{\dot{\gamma}} &= \frac{\hat{U}_0}{\hat{D}}\dot{\gamma} & \hat{\tau} &= \frac{\hat{\mu}\hat{U}_0}{\hat{D}}\tau
\end{aligned}$$

Substituting these rescaled variables into the momentum equations yields

$$\delta Re(\frac{\partial u}{\partial t} + u\frac{\partial u}{\partial x} + v\frac{\partial u}{\partial y}) = -\frac{\partial p}{\partial x} + \delta^2\frac{\partial}{\partial x}\tau_{xx} + \frac{\partial}{\partial y}\tau_{xy}, \tag{2.25}$$

$$\delta^3 Re(\frac{\partial v}{\partial t} + u\frac{\partial v}{\partial x} + v\frac{\partial v}{\partial y}) = -\frac{\partial p}{\partial y} + \delta^2\frac{\partial}{\partial x}\tau_{xy} + \delta^2\frac{\partial}{\partial y}\tau_{yy}, \tag{2.26}$$

$$\frac{\partial u}{\partial x} + \frac{\partial v}{\partial y} = 0. \tag{2.27}$$

The dimensionless small parameter δ is defined by

$$\delta \equiv \frac{\hat{D}}{\hat{L}}, \tag{2.28}$$

and Re is given by (2.17). δ will play the roll of an asymptotically small parameter in the analysis to come.

The stress/strain relationship, rate-of-strain tensor and the deviatoric stress tensor are still given by (2.18) - (2.22), but the definitions of their second invariants are now

$$\dot{\gamma} = (\dot{\gamma}_{xy}^2 + \delta^2 \dot{\gamma}_{xx}^2)^{\frac{1}{2}}, \tag{2.29}$$

and

$$\tau = (\tau_{xy}^2 + \delta^2 \tau_{xx}^2)^{\frac{1}{2}}. \tag{2.30}$$

This scaling will let us use a perturbation expansion with δ as the small parameter to analytically study the flow.

Chapter 3
Numerical Solution

We describe here the background to the algorithm used to generate the results in Chapter 4. Since the focus is on the effects of the geometry on the flow, and in particular on the formation of the plug region, we consider only a Stokes flow (i.e. the inertial terms are neglected in the momentum equations). Furthermore, we assume that the channel is periodic in the x-direction and consider only one period of the channel: $x \in [-L/2, L/2]$. The flow domain is shown in, Fig. 3.1.

For this chapter it is very convenient to write the velocity components in a subscripted manner, i.e. $\mathbf{u} = \langle u_1, u_2 \rangle$. The spatial components are also written using subscripts $\mathbf{x} = \langle x_1, x_2 \rangle$. This notation is only used in this chapter.

We begin the analysis with the classical formulation of the problem. We take the non-dimensional 2-D Stokes equations, and the Bingham constitutive model detailed in Chapter 2 which were

$$0 = -\frac{\partial p}{\partial x} + \frac{\partial}{\partial x}\tau_{xx} + \frac{\partial}{\partial y}\tau_{xy}, \tag{3.1}$$

$$0 = -\frac{\partial p}{\partial y} + \frac{\partial}{\partial x}\tau_{xy} + \frac{\partial}{\partial y}\tau_{yy}, \tag{3.2}$$

$$0 = \nabla \cdot \mathbf{u}, \tag{3.3}$$

$$\tau_{ij} = (1 + \frac{B}{\dot{\gamma}})\dot{\gamma}_{ij} \iff \quad \tau > B, \tag{3.4}$$

$$\dot{\gamma} = 0 \iff \quad \tau \leq B,$$

$$\dot{\gamma}_{ij} \equiv \frac{\partial u_i}{\partial x_j} + \frac{\partial u_j}{\partial x_i}. \tag{3.5}$$

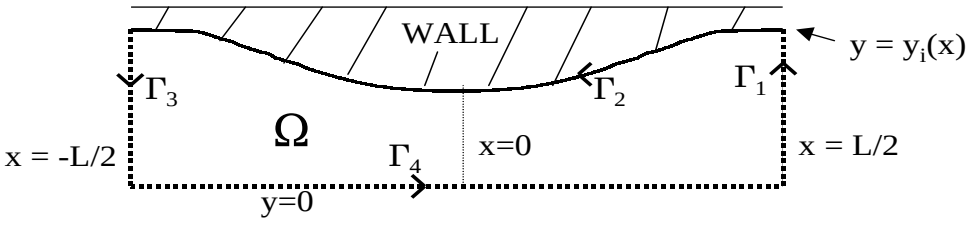

Figure 3.1: A sketch of the half-gap under consideration. $\Gamma_1, \Gamma_2, \Gamma_3$ and Γ_4 are the contours making up the boundary of the domain Ω.

The boundary conditions imposed on $\mathbf{u}$ and $\tau_{ij}(\mathbf{u})$ are the following:

$$u_2 = 0, \quad \tau_{xx} = 0, \quad \text{on } \Gamma_1 \equiv \; x = L/2, \; y \in (0, y_i(L/2)), \tag{3.6}$$

$$u_1 = 0, \quad u_2 = 0, \quad \text{on } \Gamma_2 \equiv \; x \in [-L/2, L/2], \; y = y_i(x), \tag{3.7}$$

$$u_2 = 0, \quad \tau_{xx} = 0, \quad \text{on } \Gamma_3 \equiv \; x = -L/2, \; y \in (0, y_i(-L/2)), \tag{3.8}$$

$$u_2 = 0, \quad \tau_{xy} = 0, \quad \text{on } \Gamma_4 \equiv \; x \in [-L/2, L/2], \; y = 0. \tag{3.9}$$

We note that the periodicity conditions on $\mathbf{u}$ at $x = \pm L/2$ have been replaced by (3.6) & (3.8), and this requires some explanation. In fact, for a Newtonian fluid, conditions such as (3.6) & (3.8) result purely from symmetry and can also be imposed at any of the positions $x = nL/2$, n an integer, as we argue below as long as $y_i(x)$ has maxima at $x = nL/2$.

First, (for either Bingham or Newtonian fluid), we assume that there exists a unique solution $\mathbf{u}$ to the classical problem with periodicity conditions. Then we may replace the boundary conditions on $\mathbf{u}$ by their negative and we find that

$$\mathbf{u}^{reverse} = -\mathbf{u},$$

is the unique solution to this reversed problem, (note that the pressure gradients are reversed). This is the classical result of Stokes flow, e.g. see [3]. Now, since the geometry of the domain is symmetric, we can simply reflect the domain about $x = 0$, impose the same boundary conditions and we find a new solution $\mathbf{u}^{reflect}$ to this problem. However, since the geometry is exactly the

same as before, we know that

$$\mathbf{u}^{reflect} = \mathbf{u}.$$

Equally, we can see that the problem for $\mathbf{u}^{reflect}$ is exactly that for $\mathbf{u}^{reverse}$ but with the geometry and boundary conditions reversed. Thus, we have:

$$u_1(x,y) = u_1^{reflect}(x,y) = -u_1^{reverse}(-x,y) = u_1(-x,y),$$

and

$$u_2(x,y) = u_2^{reflect}(x,y) = u_2^{reverse}(-x,y) = -u_2(-x,y).$$

From this we see that $u_2(0,y) = 0$ and $\dfrac{\partial}{\partial x}u_1(0,y) = 0$. Now, simply by shifting the coordinates to $x = nL/2$, n an integer, we can repeat the above argument. For a Newtonian fluid this suffices, but for a Bingham fluid we need note that $u_x = 0$ does not necessarily imply that $\tau_{xx} = 0$, except where yielded. However, if we suppose for example that the model is regularized, (e.g. by a biviscosity model), then it is clear that $\tau_{xx} = 0$.

Now we note that the symmetry argument is still stronger (at least for a Newtonian fluid). Taking higher derivatives, we see that at any point $x = nL/2$, n an integer, we have that:

$$\frac{\partial}{\partial x}\dot{\gamma}_{xy} = \frac{\partial^2}{\partial x \partial y}u_1 + \frac{\partial^2}{\partial x^2}u_2 = 0,$$

$$\frac{\partial}{\partial y}\dot{\gamma}_{yy} = 2\frac{\partial^2}{\partial y^2}u_2 = 0.$$

Extending this to the Bingham fluid by assuming that

$$\frac{\partial}{\partial x}\tau_{xy} = 0, \qquad \frac{\partial}{\partial y}\tau_{yy} = 0.$$

at $x = nL/2$, n an integer, we can evaluate the y-momentum equation and have that

$$\frac{\partial p}{\partial y}(\pm L/2, y) = 0. \tag{3.10}$$

Thus, at the ends of the domain we will also assume that p is independent of y. This will be used below in deriving our variational formulation.

3.1 Weak Variational Formulation

3.1.1 Derivation of the Functional to be Minimized

We assume that there exists a unique solution $\mathbf{u}$ to the classical problem derived above, in a weak sense which we define below. The solution $\mathbf{u} \in \bar{\mathcal{V}}$, where $\bar{\mathcal{V}}$ is the closure of $\mathcal{V}$ with respect to the $H^1(\Omega)$ norm, i.e.

$$||\mathbf{v}||_{H^1(\Omega)} = \left[\int_\Omega v_i v_i + \left(\frac{\partial v_i}{\partial x_j} \right)^2 \, d\mathbf{x} \right]^{1/2}.$$

Here Ω denotes the flow domain and $\mathcal{V}$ is defined by:

$$\mathcal{V} \quad = \quad \{\mathbf{v} \in [C^\infty(\Omega)]^2 : \ \nabla \cdot \mathbf{v} = 0 \in \Omega; \ v_2 = 0 \text{ on } \Gamma_1, \ \Gamma_3, \ \Gamma_4; \mathbf{v} = 0 \text{ on } \Gamma_2, \}. \tag{3.11}$$

In deriving the variational formulation from the classical formulation, we assume that $\mathbf{u}, \mathbf{v} \in \mathcal{V}$ and whatever other regularity is implicit (e.g. for pressure and stress fields).

The stress is defined as

$$\sigma_{ij} \equiv -p\delta_{ij} + \tau_{ij}, \tag{3.12}$$

where $\delta_{ij} = 1$ if $i = j$, otherwise $\delta_{ij} = 0$. The momentum equations, (3.1) and (3.2), written in terms of the stress, σ_{ij}, take on the simplified form

$$\frac{\partial \sigma_{ij}}{\partial x_j} = 0. \tag{3.13}$$

(Recall that it is assumed that anytime we see a repeated subscript, summation over that subscript is implicit.) Typically the pressure is only defined uniquely up to a constant, say p_0. It follows from (3.10) that the pressure experiences a constant pressure drop along the channel, say ΔP. Thus, we write p as:

$$p = p_0 - \frac{\Delta P}{L} x + \tilde{p}, \tag{3.14}$$

where we choose p_0 such that the modified pressure field $\tilde{p}$ satisfies:

$$\tilde{p}(\pm L/2, y) = 0. \tag{3.15}$$

Multiply (3.13) by $u_i - v_i$ and integrate over Ω to get

$$\int_\Omega (u_i - v_i)\frac{\partial}{\partial x_j}[-\tilde{p}\delta_{ij} + \tau_{ij}] + \frac{\Delta P}{L}(u_1 - v_1)\ d\mathbf{x} = 0. \tag{3.16}$$

Using the product rule for derivatives we get

$$\int_\Omega \frac{\partial}{\partial x_j}[(u_i - v_i)(-\tilde{p}\delta_{ij} + \tau_{ij})] - (-\tilde{p}\delta_{ij} + \tau_{ij})\frac{\partial}{\partial x_j}[u_i - v_i] + \frac{\Delta P}{L}(u_1 - v_1)\ d\mathbf{x} = 0. \tag{3.17}$$

For now, focus on the first term in (3.17). Applying Green's Theorem results in a boundary integral on $\partial\Omega$:

$$\begin{aligned} &-\int_\Omega \frac{\partial}{\partial x_j}[(v_i - u_i)(-\tilde{p}\delta_{ij} + \tau_{ij})] \\ &\quad = \oint_{\partial\Omega} \langle (-\tilde{p}\delta_{i2} + \tau_{i2})(v_i - u_i)\ ,\ -(-\tilde{p}\delta_{i1} + \tau_{i1})(v_i - u_i)\rangle \cdot d\mathbf{r} \equiv I_{\partial\Omega}. \end{aligned}$$

When the boundary integral, $I_{\partial\Omega}$, is broken up into its 4 components (one from each edge) and the essential boundary conditions for $\mathbf{u}$ (and $\mathbf{v}$) are applied we are left with

$$\begin{aligned} I_{\partial\Omega} \quad = \quad & \left\{ -\int_0^{y_i} (-\tilde{p} + \tau_{11})(v_1 - u_1)|_{x=1/2}\, dy - \int_{y_i}^{0} (-\tilde{p} + \tau_{11})(\mathbf{u})(v_1 - u_1)|_{x=-1/2}\, dy \right. \\ & \left. + \int_{-L/2}^{L/2} \tau_{xy}(v_1 - u_1)|_{y=0}\, dx \right\}. \end{aligned} \tag{3.18}$$

Now, we see that these remaining terms vanish due to the *non-essential* conditions in (3.6), (3.8) & (3.9) and due to the *non-essential* condition (3.15) on $\tilde{p}$ at the ends of the channel section.

Thus, returning to (3.17) and noting that functions in $\mathcal{V}$ are divergence free, we have

$$\int_\Omega \tau_{ij}\frac{\partial}{\partial x_j}[v_i - u_i]\ d\mathbf{x} = \frac{\Delta P}{L}\int_\Omega (v_1 - u_1)\ d\mathbf{x}, \tag{3.19}$$

and using the symmetry of τ_{ij} we rewrite (3.19) as

$$\int_\Omega \frac{1}{2}\dot{\gamma}_{ij}(\mathbf{v} - \mathbf{u})\tau_{ij}\ d\mathbf{x} = \frac{\Delta P}{L}\int_\Omega (v_1 - u_1)\ d\mathbf{x}. \tag{3.20}$$

We now derive an inequality by considering the first term in (3.20). We consider separately and pointwise, regions in which $\tau > B$ and those in which $\tau \leq B$. First, using the definition of τ_{ij}

for $\tau > B$ gives

$$\begin{aligned}\int_\Omega \frac{1}{2}\tau_{ij}(\mathbf{u})\dot{\gamma}_{ij}(\mathbf{v}-\mathbf{u}) &= \int_\Omega \left(1+\frac{B}{\dot{\gamma}(\mathbf{u})}\right)\frac{1}{2}\dot{\gamma}_{ij}(\mathbf{u})\dot{\gamma}_{ij}(\mathbf{v}-\mathbf{u}) \\ &= \int_\Omega \frac{1}{2}\dot{\gamma}_{ij}(\mathbf{u})\dot{\gamma}_{ij}(\mathbf{v}-\mathbf{u}) + B\int_\Omega \frac{\frac{1}{2}\dot{\gamma}_{ij}(\mathbf{u})\dot{\gamma}_{ij}(\mathbf{v})}{\dot{\gamma}(\mathbf{u})} - \dot{\gamma}(\mathbf{u}).\end{aligned}$$

The Cauchy-Schwarz inequality tells us

$$\frac{1}{2}\dot{\gamma}_{ij}(\mathbf{u})\dot{\gamma}_{ij}(\mathbf{v}) \leq \dot{\gamma}(\mathbf{u})\dot{\gamma}(\mathbf{v}).$$

We now have for $\tau(\mathbf{u}) > B$:

$$\int_\Omega \frac{1}{2}\sigma_{ij}(\mathbf{u})\dot{\gamma}_{ij}(\mathbf{v}-\mathbf{u}) \leq \int_\Omega \frac{1}{2}\dot{\gamma}_{ij}(\mathbf{u})\dot{\gamma}_{ij}(\mathbf{v}-\mathbf{u}) + B\int_\Omega \dot{\gamma}(\mathbf{v}) - \dot{\gamma}(\mathbf{u}). \tag{3.21}$$

For $\tau \leq B$ we do not have an explicit expression for τ_{ij} like we did for $\tau > B$. However, we shall see that inequality (3.21) remains true. If $\tau \leq B$, we know $\dot{\gamma}_{ij}(\mathbf{u}) = 0$ and $\dot{\gamma}(\mathbf{u}) = 0$, so

$$\frac{1}{2}\tau_{ij}(\mathbf{u})\dot{\gamma}_{ij}(\mathbf{v}-\mathbf{u}) = \frac{1}{2}\tau_{ij}(\mathbf{u})\dot{\gamma}_{ij}(\mathbf{v}).$$

Again, the Cauchy-Schwartz inequality can be used to get the result

$$\frac{1}{2}\tau_{ij}(\mathbf{u})\dot{\gamma}_{ij}(\mathbf{v}) \leq \tau(\mathbf{u})\dot{\gamma}(\mathbf{v}).$$

Therefore, for the case where $\tau \leq B$, we have

$$\int_\Omega \frac{1}{2}\sigma_{ij}(\mathbf{u})\dot{\gamma}_{ij}(\mathbf{v}-\mathbf{u}) \leq \int_\Omega \tau(\mathbf{u})\dot{\gamma}(\mathbf{v}) \leq B\int_\Omega \dot{\gamma}(\mathbf{v}). \tag{3.22}$$

Taking into consideration $\dot{\gamma}(\mathbf{u}) = 0$ for $\tau \leq B$ we see that in fact, equation (3.21) holds for all values of τ.

Combining with (3.20), this leads to the following weak variational formulation of the problem:

$$\int_\Omega \frac{1}{2}\dot{\gamma}_{ij}(\mathbf{u})\dot{\gamma}_{ij}(\mathbf{v}-\mathbf{u}) + B\int_\Omega \dot{\gamma}(\mathbf{v}) - \dot{\gamma}(\mathbf{u}) \geq \frac{\Delta P}{L}\int_\Omega v_1 - u_1. \tag{3.23}$$

The solution $\mathbf{u}$ is the function $\mathbf{u} \in \bar{\mathcal{V}}$ for which inequality (3.23) holds for all $\mathbf{v} \in \bar{\mathcal{V}}$. We assume that such a function can be found. It follows that $\mathbf{u}$ will also minimize the functional

$$\mathcal{J}(\mathbf{v}) = \int_\Omega \frac{1}{2}\dot{\gamma}^2(\mathbf{v}) + B\int_\Omega \dot{\gamma}(\mathbf{v}) - \frac{\Delta P}{L}\int_\Omega v_1. \tag{3.24}$$

3.1.2 Determining ΔP

Note that the solution that we require is in fact the pair $(\mathbf{u}, \Delta P)$. We have scaled the velocity with the mean velocity through the channel and therefore should have that

$$\int_0^{y_i} u_1 dy = 1,$$

at any point x. By differentiating this integral with respect to x and using the incompressibility condition, we see that there is no x variation in the above integral.

$$\frac{\partial}{\partial x}\int_0^{y_i} u_1 dy = u_1(x, y_i)\frac{dy_i}{dx} + \int_0^{y_i} \frac{\partial}{\partial x} u_1 dy = -\int_0^{y_i} \frac{\partial}{\partial y} u_2 dy = 0.$$

Thus, our flow rate constraint above can be written as:

$$\frac{1}{L}\int_\Omega u_1 d\mathbf{x} = 1, \tag{3.25}$$

which corresponds to the linear functional in (3.23). The question now is whether we can find a constant ΔP such that (3.25) is always satisfied.

We can see this is the case by using (3.23). Denote by $\mathbf{u}_{\Delta P}$ the solution of (3.23) corresponding to pressure drop ΔP, and suppose we have $\Delta P_2 > \Delta P_1$. It is clear that $\mathbf{u}_{\Delta P_1}$ is a test function for $\mathbf{u}_{\Delta P_2}$ and vice versa. Substituting these functions for $\mathbf{v}$ in (3.23) for the two solutions, and summing gives:

$$0 \leq \int_\Omega \dot{\gamma}^2(\mathbf{u}_{\Delta P_1} - \mathbf{u}_{\Delta P_2}) d\mathbf{x} \leq \frac{(\Delta P_2 - \Delta P_1)}{L}\int_\Omega \mathbf{u}_{\Delta P_2,1} - \mathbf{u}_{\Delta P_1,1} d\mathbf{x}.$$

Thus, we see that the integral in (3.25), effectively the flow rate, increases monotonically with the pressure drop. Indeed, provided that $\Delta P_2 > \Delta P_1$ and $\mathbf{u}_{\Delta P_1} \neq \mathbf{u}_{\Delta P_2}$, the increase is strictly monotone. It appears therefore that we can decouple the problem for (3.25), by first solving for fixed ΔP and then iterating with respect to ΔP to satisfy (3.25).

3.1.3 The Minimization Problem

It is worth noting that the term in (3.24) containing $\dot{\gamma}(\mathbf{u})$ is non-differentiable, which causes problems for any conventional minimization. This term will require special treatment and here

we follow the approach taken by Glowinski [4]. First we relax the minimization problem, by introducing an auxiliary variable, $\mathbf{q}$. This variable will have two components, the first of which will behave like $\dot{\gamma}_{xx}(\mathbf{v})$, and the second component acting like $\dot{\gamma}_{xy}(\mathbf{v})$. Consider the following two constraints:

$$q_1 = \frac{\partial v_1}{\partial x} - \frac{\partial v_2}{\partial y} = \frac{1}{2}\dot{\gamma}_{xx}(\mathbf{v}) - \frac{1}{2}\dot{\gamma}_{yy}(\mathbf{v}), \tag{3.26}$$

$$q_2 = \frac{\partial v_1}{\partial y} + \frac{\partial v_2}{\partial x} = \dot{\gamma}_{xy}(\mathbf{v}). \tag{3.27}$$

We then replace $\dot{\gamma}(\mathbf{v})$ and $\dot{\gamma}^2(\mathbf{v})$ with $|\mathbf{q}|$ and $|\mathbf{q}|^2$ respectively. Then the minimization is taken to be over $\mathbf{v} \in \mathcal{V}$ and $\mathbf{q} \in L^2(\Omega)$, but with (3.26) and (3.27) satisfied. Then the problem is

$$\min_{\mathbf{v},\,\mathbf{q}} \mathcal{J}(\mathbf{v},\mathbf{q}) = \int_\Omega \frac{1}{2}|\mathbf{q}|^2 + B\int_\Omega |\mathbf{q}| - \frac{\Delta P}{L}\int_\Omega v_1. \tag{3.28}$$

The next step is critical. In order to relate the auxiliary variable $\mathbf{q}$ to the velocity field, penalty terms are needed. The reason for doing so is that (3.26) and (3.27) are difficult constraints to satisfy directly in a numerical discretisation. We thus relax (3.26) and (3.27) but add linear and quadratic penalty terms for these constraints. The other difficulty numerically is the incompressibility condition. This we also remove from the problem via the introduction of linear and quadratic penalty terms for the incompressibility. Thus, we consider:

$$\begin{aligned}\min_{\mathbf{v},\,\mathbf{q}}\ \max_{\lambda,\,p}\quad \mathcal{L}(\mathbf{v},\mathbf{q},\lambda,\tilde{p}) \;=\; & \int_\Omega \left\{ \frac{1}{2}|\mathbf{q}|^2 + B|\mathbf{q}| - \frac{\Delta P}{L}v_1 \right. \\ & +\lambda_1\left(\frac{\partial v_1}{\partial x} - \frac{\partial v_2}{\partial y} - q_1\right) + \lambda_2\left(\frac{\partial v_1}{\partial y} + \frac{\partial v_2}{\partial x} - q_2\right) \\ & +\frac{k_1}{2}\left[\left(\frac{\partial v_1}{\partial x} - \frac{\partial v_2}{\partial y} - q_1\right)^2 + \left(\frac{\partial v_1}{\partial y} + \frac{\partial v_2}{\partial x} - q_2\right)^2\right] \\ & \left. -\tilde{p}\nabla\cdot\mathbf{v} + \frac{k_2}{2}(\nabla\cdot\mathbf{v})^2 \right\}\, d\mathbf{x}\ .\end{aligned} \tag{3.29}$$

where λ, $\mathbf{q} \in H \equiv L^2(\Omega) \times L^2(\Omega)$ and $\tilde{p} \in L^2(\Omega)$. k_1 and k_2 are constants. And now,

$$\mathbf{v} \in \mathcal{K} \equiv \{\mathbf{w} \in [\mathrm{H}^1(\Omega)]^2 \ :\ \mathbf{w}_2 = 0 \text{ on } \Gamma_1,\ \Gamma_3,\ \Gamma_4; \mathbf{w} = 0 \text{ on } \Gamma_2\}.$$

The functional $\mathcal{L}(\mathbf{v},\mathbf{q},\lambda,\tilde{p})$ is referred to as the augmented Lagrangian functional. The variables λ_1, λ_2 and $\tilde{p}$ play the role of Lagrange multipliers for the constraints (3.26), (3.27) and

incompressibility, respectively. With $k_1 = k_2 = 0$ this functional is referred to as a Lagrangian. The Lagrangian is then augmented with the quadratic penalty terms for stability, leading to (3.30). Note that $\tilde{p}$ will in fact also play the role of the modified pressure $\tilde{p}$ introduced earlier.

3.2 Solution of Augmented Lagrangian

A solution to the augmented Lagrangian is attained by an iterative procedure of Uzawa type. This algorithm is presented in [4] as ALG 2 in §6.3. The algorithm goes as follows,

$$\{\mathbf{q}^0, \lambda^1, \tilde{p}^1\} \in H \times H \times L^2(\Omega) \text{ given :}$$

then, $\{\mathbf{q}^{n-1}, \lambda^n, \tilde{p}^n\}$ known, we define $\{\mathbf{q}^n, \lambda^{n+1}, \tilde{p}^{n+1}\}$ by:

$$\mathcal{L}(\mathbf{u}^n, \mathbf{q}^{n-1}, \lambda^n, \tilde{p}^n) \leq \mathcal{L}(\mathbf{v}, \mathbf{q}^{n-1}, \lambda^n, \tilde{p}^n) \quad \forall \mathbf{v} \in \mathcal{K}, \mathbf{u}^n \in \mathcal{K}, \tag{3.30}$$

$$\mathcal{L}(\mathbf{u}^n, \mathbf{q}^n, \lambda^n, \tilde{p}^n) \leq \mathcal{L}(\mathbf{u}^n, \mathbf{z}, \lambda^n, \tilde{p}^n) \quad \forall \mathbf{z} \in H, \mathbf{q}^n \in H, \tag{3.31}$$

$$\lambda_1^{n+1} = \lambda_1^n + \rho_1(\frac{\partial u^n}{\partial x} - \frac{\partial v^n}{\partial y} - \mathbf{q}_1^n), \tag{3.32}$$

$$\lambda_2^{n+1} = \lambda_2^n + \rho_1(\frac{\partial u^n}{\partial y} + \frac{\partial v^n}{\partial x} - \mathbf{q}_2^n), \tag{3.33}$$

$$\tilde{p}^{n+1} = \tilde{p}^n - \rho_2(\nabla \cdot \mathbf{u}^{\mathbf{n}}), \tag{3.34}$$

where $\rho_1, \rho_2 > 0$ are relaxation parameters associated with k_1 and k_2 respectively. For the computations presented in Chapter 4, we use $\rho_1 = \rho_2 = k_1 = k_2 = 1$, which seems to work well.

Glowinski [4] shows that this algorithm has the following convergence properties:

$$\begin{aligned}
\mathbf{u}^n &\longrightarrow \mathbf{u} \text{ strongly in } \mathcal{K}, \\
\mathbf{q}^n &\longrightarrow \mathbf{q} \text{ strongly in } H, \\
\lambda^{n+1} - \lambda^n &\longrightarrow 0 \text{ strongly in } H, \\
\tilde{p}^{n+1} - \tilde{p}^n &\longrightarrow 0 \text{ strongly in } L^2(\Omega), \\
\lambda^n &\text{ bounded in } H, \\
\tilde{p}^n &\text{ bounded in } L^2(\Omega).
\end{aligned}$$

To simplify the solution of (3.30), in the implementation that produced the results in Chapter 4, the individual velocity components were solved for separately in a decoupled fashion. First

u_1^n was solved for keeping u_2^{n-1} fixed, then u_2^n was solved for keeping u_1^n fixed. In essence, this simplification amounts to weakening the quadratic penalty term for the incompressibility condition, as a result, it needed more iterations to converge. However, the linear systems being solved are only half the size, which results in much faster iterations. It is also much simpler to implement.

3.2.1 The velocity subproblem

The subscript notation for velocity and spatial directions are no longer useful. The notation that we use now will be the same notation used for the remainder of the paper. It is $\mathbf{u} = \langle u, v \rangle$ and $\mathbf{x} = \langle x, y \rangle$. This notation is useful because it allows us to write partial derivatives as subscripts.

We now consider problem (3.30) for the x-component of velocity, to see what the differential form of this minimization is. Let t be a real number and $\mathbf{h} \in \mathcal{K}$ be a variation of the x-component of the velocity field. Then, if $\mathbf{u}$ is the solution to (3.30) we know that,

$$\begin{aligned} 0 &= \frac{\partial \mathcal{L}_R(u + th, v, \mathbf{q}, \lambda, \tilde{p})}{\partial t} \\ &= \left\{ \int_\Omega -\tilde{p}h_x + k_2(\nabla \cdot \mathbf{u})h_x + k_1[u_x - v_y - q_1]h_x + k_1[u_y + v_x - q_2]h_y \right. \\ &\quad \left. + \lambda_1 h_x + \lambda_2 h_y - \frac{\Delta P}{L} h \, d\mathbf{x} \right\} \\ &= \int_\Omega \nabla h \cdot \mathbf{a} - \frac{\Delta P}{L} h \, d\mathbf{x}, \end{aligned} \tag{3.35}$$

where for ease of notation,

$$\mathbf{a} \equiv \langle -\tilde{p} + k_2(u_x + v_y) + k_1[u_x - v_y - q_1] + \lambda_1 \ , \ k_1[u_y + v_x - q_2] + \lambda_2 \rangle.$$

After applying Green's Theorem, this becomes

$$0 = \oint_{\partial\Omega} \langle -a_2 h \ , \ a_1 h \rangle \cdot d\mathbf{r} - \int_\Omega h \left[\nabla \cdot \mathbf{a} + \frac{\Delta P}{L} \right] d\mathbf{x}. \tag{3.36}$$

Thus, since h is any admissible variation, we know that,

$$\begin{aligned} 0 &= \nabla \cdot \mathbf{a} + \frac{\Delta P}{L} \\ &= k_1 \nabla^2 u + k_2 u_{xx} + \nabla \cdot \langle k_2 v_y - \tilde{p} - k_1 q_1 + \lambda_1 \ , \ \lambda_2 - k_1 q_2 \rangle + \frac{\Delta P}{L} \\ &\equiv k_1 \nabla^2 u_1 + k_2 u_{xx} + \nabla \cdot \mathbf{f} + \frac{\Delta P}{L}, \end{aligned} \tag{3.37}$$

everywhere in the interior domain of Ω. In the final formulation of the finite element equations for u, there will be the natural conditions $\dfrac{\partial u}{\partial n} = 0$ on the ends of Ω and the centerline, $y = 0$.

We now use the same method to derive an explicit differential form for v. Begin by taking a variation h about the second velocity component, v, using homogeneous boundary conditions for h on all boundaries:

$$\begin{aligned} 0 &= \frac{\partial \mathcal{L}_R(u, v + th, \mathbf{q}, \lambda, \tilde{p})}{\partial t} \\ &= \Big\{ \int_\Omega -\tilde{p} h_y + k_2 (\nabla \cdot \mathbf{u}) h_y - k_1 [u_x - v_y - q_1] h_y + k_1 [u_y + v_x - q_2] h_x \\ &\quad -\lambda_1 h_y + \lambda_2 h_x \, d\mathbf{x} \Big\} \\ &= \int_\Omega \nabla h \cdot \mathbf{b} \, d\mathbf{x}, \end{aligned} \tag{3.38}$$

where $\mathbf{b}$ is given by

$$\mathbf{b} \equiv \langle k_1 (u_y + v_x - q_2) + \lambda_2 \ , \ -\tilde{p} + k_2 (u_x + v_y) - k_1 (u_x - v_y - q_1) - \lambda_1 \rangle.$$

Again, we apply Green's Theorem. This time the homogeneous conditions on h leave

$$0 = \int_\Omega h (\nabla \cdot \mathbf{b}) \, d\mathbf{x}. \tag{3.39}$$

This is true for any h satisfying the boundary conditions, so we can conclude,

$$\begin{aligned} 0 &= k_1 \nabla^2 v + k_2 v_{yy} + \nabla \cdot \langle \lambda_2 - k_1 q_2 \ , \ k_2 u_x - \tilde{p} - \lambda_1 + k_1 q_1 \rangle \\ &\equiv k_1 \nabla^2 v + k_2 v_{yy} + \nabla \cdot \mathbf{g}, \end{aligned} \tag{3.40}$$

everywhere in the interior of Ω.

As mentioned earlier, (3.37) and (3.40) will be solved in a decoupled manner. First (3.37) will be solved using v^{n-1} to evaluate $\mathbf{f}$. Then (3.40) will be solved using u^n to evaluate $\mathbf{g}$.

3.2.2 The q sub-problem

If we have some fixed, $\mathbf{u}^n$, λ^n and $\tilde{p}^n$ and we only allow $\mathbf{q}$ to vary, we see our minimization problem becomes

$$\min_{\mathbf{q}} \quad \mathcal{L}(\mathbf{q}) = \frac{1}{2}\int_\Omega |\mathbf{q}|^2 + B\int_\Omega |\mathbf{q}| + \frac{k_1}{2}\int_\Omega |\mathbf{q}|^2 - \int_\Omega \mathbf{C}\cdot\mathbf{q}, \tag{3.41}$$

where

$$\mathbf{C} \equiv \langle \lambda_1 + k_1(u_x - v_y)\ ,\ \lambda_2 + k_1(u_y + v_x)\rangle.$$

We will see in §1 of Chapter 4 that when we choose bilinear elements for u and v, that the proper choice of basis for λ_1, λ_2 and $\tilde{p}$ are piecewise constant on each element. The updates (3.32)-(3.34) are then performed in an average sense over the element, which is equivalent to evaluating the velocity derivatives at the centroid of the element. All this implies that q_1 and q_2 should also be piecewise constant on each element, and the velocity derivatives in $\mathbf{C}$ should be evaluated at the centroid of the element. With this scheme, the relationships (3.26)-(3.27) between $\mathbf{q}$ and $\dot{\gamma}_{ij}$ hold in an average sense over each element, and are satisfied exactly at the centroid of each element. This means that the minimization for $\mathbf{q}$ discussed here can be done separately over each individual element, which makes the solution of (3.41) simple.

It is obvious from looking at (3.41) that for any fixed length of $\mathbf{q}$, $\mathcal{L}$ will be minimized when $\mathbf{q}$ points in the same direction as $\mathbf{C}$, i.e. $\mathbf{q} = d\mathbf{C}$, where d is a non-negative real. Therefore, we can reduce this minimization to the following 1-D problem, (where it is implicit that we minimize on each element):

$$\min_{d \geq 0} \quad \mathcal{L}_A(d) = \frac{1+k_1}{2}|\mathbf{C}|^2 d^2 + (B|\mathbf{C}| - |\mathbf{C}|^2)d. \tag{3.42}$$

Immediately we see that if $B \geq |\mathbf{C}|$, then $d = 0$ and $\mathbf{q} = 0$.

However, for the case $B < |\mathbf{C}|$, we differentiate the integrand and set the result equal to zero to find

$$\begin{aligned} d &= \frac{1 - \frac{B}{|\mathbf{C}|}}{1+k_1} > 0, \\ \mathbf{q} &= d\ \mathbf{C}. \end{aligned} \tag{3.43}$$

Chapter 4
Numerical Results

4.1 Notes on Numerical Implementation

For implementation, we represent u and v with bilinear quadrilateral basis functions, i.e. $u = \sum u_j N_j$ and $v = \sum v_j N_j$ where N_j is piecewise bilinear. To obtain the element equations, we multiply both sides of (3.37) by an arbitrary basis function, N_i, integrate over a single element and write u and v as a sum of basis functions, giving

$$\sum_j \int_{\Omega_E} u_j(k_1 \nabla^2 N_j N_i + k_2 N_{j,xx} N_i)\, d\mathbf{x} = -\int_{\Omega_E} \nabla \cdot \mathbf{f} N_i \, d\mathbf{x} - \int_{\Omega_E} \frac{\Delta P}{L}\, d\mathbf{x}, \tag{4.1}$$

where $\mathbf{f} = \langle k_2 v_y - \tilde{p} - k_1 q_1 + \lambda_1 \ , \ \lambda_2 - k_1 q_2 \rangle$.

The form of this equation suggests that the appropriate basis functions for p, λ_1, λ_2, q_1 and q_2 are constant on each element. This is because we want $\nabla \cdot \mathbf{f} \sim \nabla^2 N_j$, and N_j is bilinear. Now we use Green's Theorem on both sides to get the final form of the element matrix equations arising from the variation of u:

$$\int_{\Omega_E} \sum_j u_j(k_1 \nabla N_j \cdot \nabla N_i + k_2 N_{j,x} N_{i,x})\, d\mathbf{x} = -\int_{\Omega_E} \mathbf{f} \cdot \nabla N_i \, d\mathbf{x} + \int_{\Omega_E} \frac{\Delta P}{L}\, d\mathbf{x}. \tag{4.2}$$

The natural condition $\dfrac{\partial u}{\partial n}$ arising from symmetry is used to eliminate the boundary integral arising from this use of Green's Theorem.

The same procedure is used to arrive at the following element equation for v:

$$\int_{\Omega_E} \sum_j v_j(k_1 \nabla N_j \cdot \nabla N_i + k_2 N_{j,y} N_{i,y})\, d\mathbf{x} = -\int_{\Omega_E} \mathbf{g} \cdot \nabla N_i \, d\mathbf{x}, \tag{4.3}$$

where $\mathbf{g} = \langle \lambda_2 - k_1 q_2 \ , \ k_2 u_x - \tilde{p} - \lambda_1 + k_1 q_1 \rangle$.

As mentioned in Chapter 3, to have the correct numerical solution we need to choose a constant mean pressure drop, ΔP, that yields a unit flow rate across the gap half-width. To find this ΔP, we implement an outer-loop around the solution of the augmented Lagrangian, i.e. first we solve the augmented Lagrangian with an approximate ΔP^n, and then we choose ΔP^{n+1} according to the flow rate given by the velocity field (recall the flow rate is monotonically related to the mean pressure drop). This process is repeated until the resulting flow rate across the gap half-width is within an acceptable tolerance range. To ensure this procedure works well, the outer-loop should only occur once the augmented Lagrangian has iterated enough to give a good approximation of the converged flow rate. In practice, it only took 4 or 5 iterations of ΔP to get an acceptable solution.

4.2 Error in a Straight Channel

When there is no variation in the gap width, we know the analytical solution to the problem (it is developed in Chapter 5). We use this for a test problem to see how the element size affects the L^2 norm of the velocity error. We calculate on a computational domain that is a 1 unit by 1 unit square (this corresponds to a channel with periodic length 2 and gap half-width 1) and let k denote the number of elements in either direction (we use a uniform square mesh).

It is worth noting that when there is no variation in gap width that the solution is fully converged after only two iterations of the augmented Lagrangian.

k	L^2(error)
10	.00581103
20	.00146366
40	.00040736
60	.000245451
80	.000131523
100	.0000631973
120	.0000401938

Table 4.1: A table showing the relationship between grid resolution (k elements in each direction) and the L^2 velocity error norm.

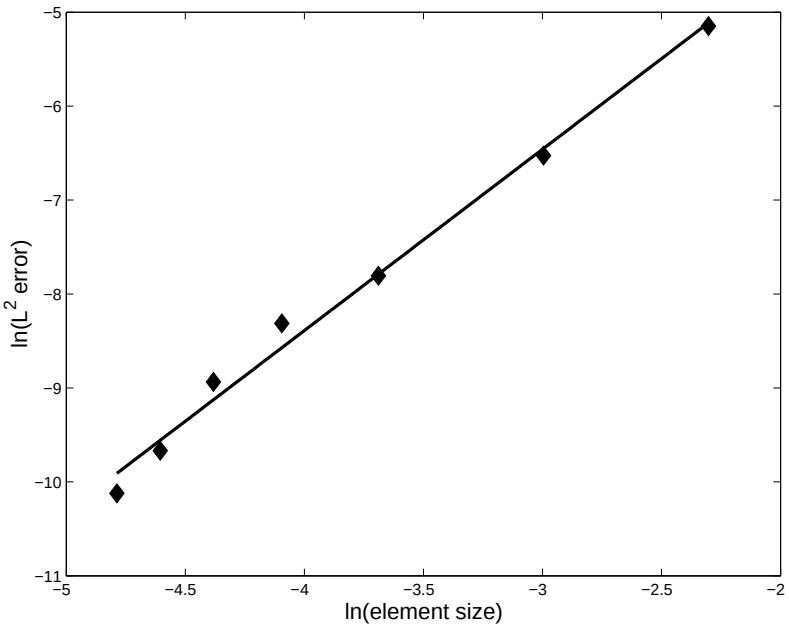

Figure 4.1: A plot of the logarithm of the element size $\equiv \overline{h}$ vs. the logarithm of the L^2 velocity error norm. The line shown is found by a least-squares approximation, and has slope ≈ 1.93. This suggests that $L^2(\text{velocity error}) \sim \mathcal{O}(\overline{h}^2)$ for the straight channel problem.

n	$L^2(u^n - u^{n-1})$	$L^2(\lambda_1^{n+1} - \lambda_1^n)$	$L^2(\lambda_2^{n+1} - \lambda_2^n)$	$L^2(p^{n+1} - p^n)$
50	3.95292 e -4	.00524789	.00163119	.00737470
100	1.13832 e -4	.00159296	5.63465 e -4	.00218611
150	3.09011 e -5	5.15219 e -4	1.95149 e -4	6.75485 e -4
200	9.55098 e -6	2.11226 e -4	8.15549 e -5	2.58076 e -4

Table 4.2: A table illustrating the convergence of the augmented Lagrangian. The parameters $B = 5, h = .05$ and $L = 4$ were used to generate these results.

4.3 Results for Varying Gap Width

Table 4.2 gives an idea of how well the augmented Lagrangian converges. We see that the L^2 norms of

$$(u^n - u^{n-1}), \quad (\lambda_1^{n+1} - \lambda_1^n), \quad (\lambda_2^{n+1} - \lambda_2^n), \text{and} \quad (p^{n+1} - p^n)$$

all converge to zero as $n \longrightarrow \infty$. Because of how we update λ_1, λ_2 and p, this means that

$$(u_x^n - v_y^n - q_1^n), \quad (u_y^n + v_x^n - q_2^n), \text{and} \quad \nabla \cdot \mathbf{u}$$

converge to zero as $n \longrightarrow \infty$. Thus we see that $\mathbf{u}$ is indeed converging to the solution of the original problem.

If the velocity components were solved in a coupled fashion (as shown in (3.30)) then it would surely take fewer iterations to get convergence of the augmented Lagrangian. However, by decoupling the velocity problem, the size of the linear system is halved, which results in a much faster solution of the system.

Experimentally, it has been the case that a higher Bingham number results in slower convergence of the algorithm, i.e. more iterations are needed.

Figs. 4.2 - 4.8 are two color plots of the plug regions for various choices of B, h and L. The grey regions indicate where the fluid is yielded and the black regions indicate the unyielded

plug regions. Fig. 4.2 can be considered a base case. Then Figs. 4.3-4.4 vary B, Figs. 4.5-4.6 vary h, and Figs. 4.7-4.8 vary L.

We see that in the base case, where $B = 5$, an unbroken plug exists along the length of the gap. When we leave h and L unchanged and choose $B = 1$ (see Fig. 4.3), we see that the plug has broken into two plug regions separated by a stretch of fully yielded fluid. This seems intuitive as lowering B amounts to reducing the effective yield strength of the fluid. When B is increased to 20 (see Fig. 4.4), we see that there is an unbroken plug and in fact the plug region has increased in size compared to the base case. Again this seems intuitive as the effective yield strength of the fluid has been increased. This implies that the plug is more likely to remain intact for larger values of B. Also, for larger values of B we expect the yield surface to move out further towards the wall.

Now, to investigate the effects of varying the amplitude of the wall variation, we refer to Figs. 4.5 and 4.6. In the base case, $h = .085$ is used. In Fig. 4.5 we decrease this value to $h = .05$. We see that when compared to the base case, the yield surface takes a different shape. The yield surface in Fig. 4.5 has less of a dip around $x = -1/4$ when compared to the yield surface in the base case. This could be understood by considering the size of $|\tau_{xx}|$. When the slope of the gap wall is increased, the size of $|\tau_{xx}|$ should increase as well. So, when we decrease the size of h, we have decreased the slope of the gap wall, especially in the region around $x = -1/4$. As a result the plug has increased in size around this region. When we increase the size of h, we would be increase the size of $|\tau_{xx}|$ in this region. Looking at Fig. 4.6 we see that this is what appears to have happened, as now the plug region has broken into two separate plugs. This means that $|\tau|$ has now exceeded the yield value around the region $x = -1/4$. This implies that the plug is more likely to remain intact for lower values of h.

Lastly we consider the effect of the parameter L. In the base case we have $L = 4$. In Figs. 4.7 and 4.8 we use $L = 10$ and $L = 20$ respectively. We see that in both cases the plug has now broken into two separate plug regions. It does not appear that there is much of a difference between Fig. 4.7 and Fig. 4.8, however, looking closely we see that the size of the plug regions

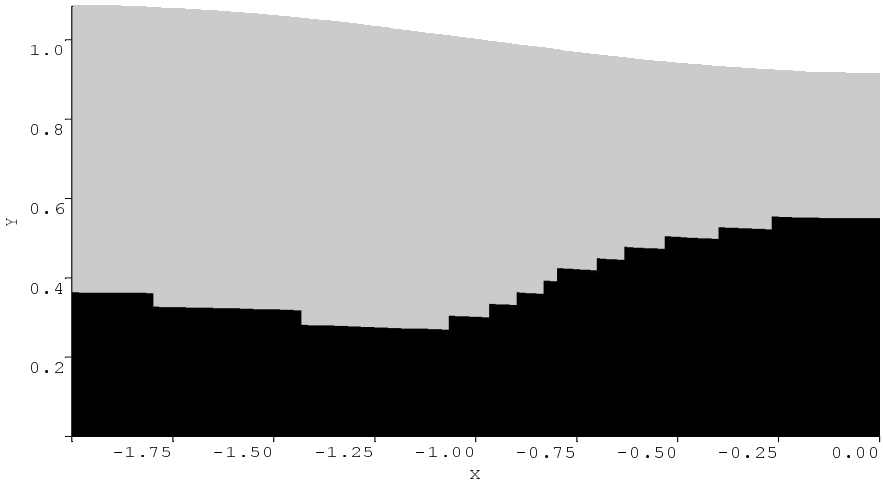

Figure 4.2: A two color plot of the plug region with $B = 5, h = .085, L = 4$. The plug region is shown in black and the yielded region is shaded gray.

differ very slightly. The most we can really conclude from these runs is that the plug is more likely to break when L is a larger value.

We will see in Chapters 5 and 6 that all of the general conclusions reached here agree with the analytical results (when the Bingham number is not large, as this causes the asymptotic results to break down).

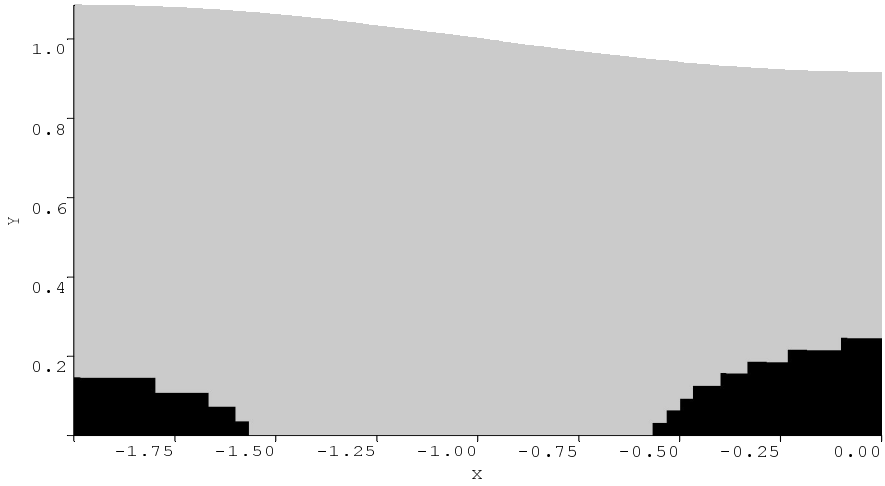

Figure 4.3: A two color plot of the plug region with $B = 1, h = .085, L = 4$. The plug region is shown in black and the yielded region is shaded gray.

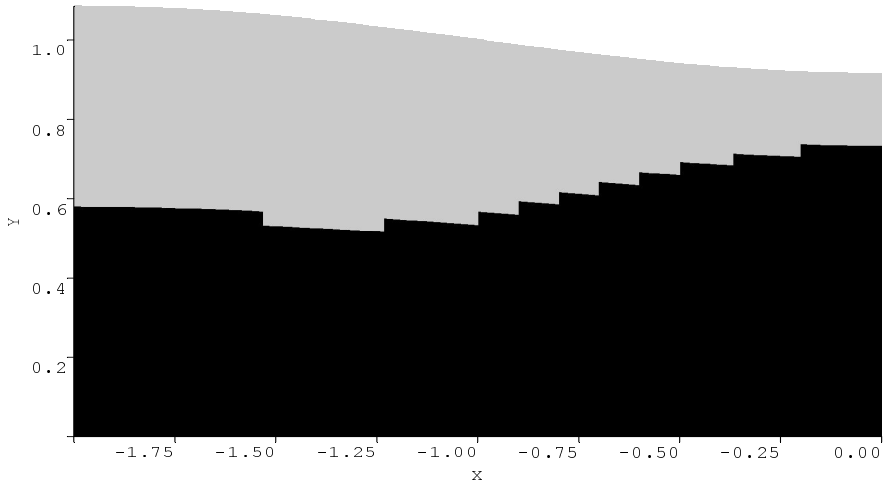

Figure 4.4: A two color plot of the plug region with $B = 20, h = .085, L = 4$. The plug region is shown in black and the yielded region is shaded gray.

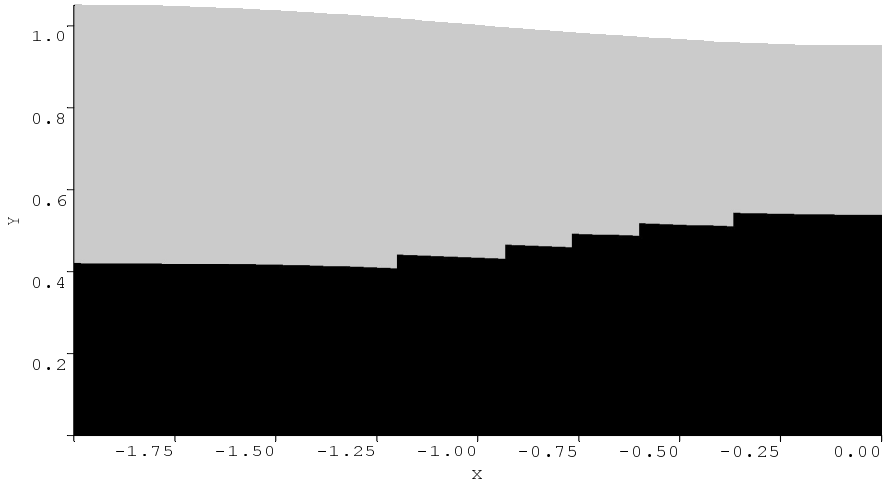

Figure 4.5: A two color plot of the plug region with $B = 5, h = .05, L = 4$. The plug region is shown in black and the yielded region is shaded gray.

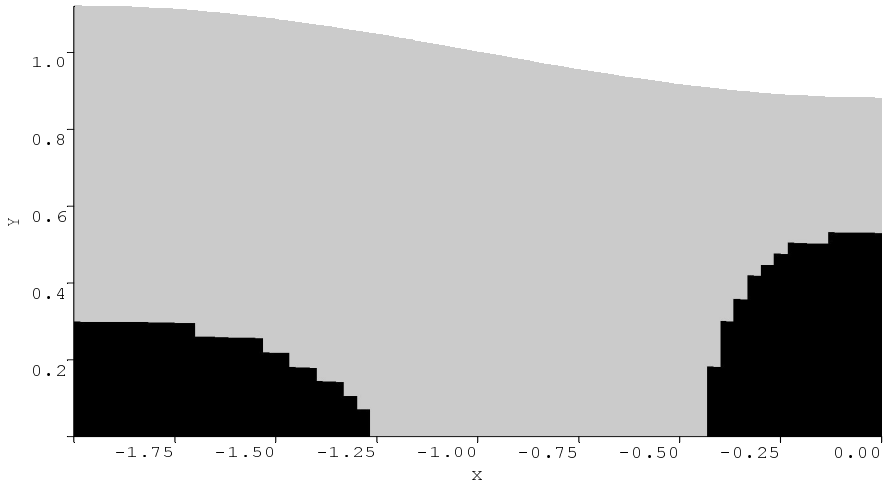

Figure 4.6: A two color plot of the plug region with $B = 5, h = .12, L = 4$. The plug region is shown in black and the yielded region is shaded gray.

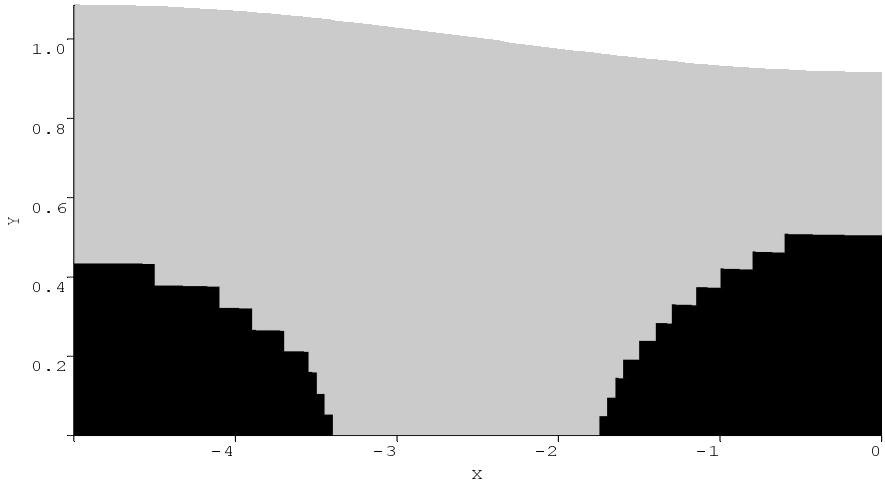

Figure 4.7: A two color plot of the plug region with $B = 5, h = .085, L = 10$. The plug region is shown in black and the yielded region is shaded gray.

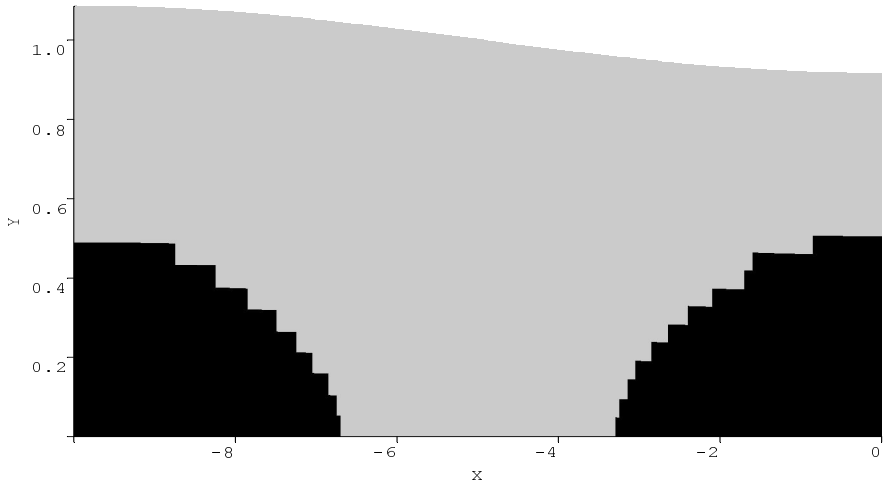

Figure 4.8: A two color plot of the plug region with $B = 5, h = .085, L = 20$. The plug region is shown in black and the yielded region is shaded gray.

Taking cross-sections of the u_1 velocity component at various points along the channel will let us see what is happening more clearly. Fig. 4.9 shows cross-sections at $x = -L/2, x = -L/4$, and $x = 0$ for the case $B = 5, h = .05$ and $L = 4$ (note the plug region for this set of parameters was shown in Fig. 4.5). We see that the plug is indeed moving at a uniform speed.

Looking at Fig. 4.10 we see that the cross-section taken at $x = -L/4$ has no plug region, and the cross-sections taken at $x = 0$ and $x = -L/2$ both have plug regions, but they have different plug speeds. This is consistent with Fig. 4.8 which shows that the plug has broken into two separate plugs and there is a region around $x = -L/4$ where no plug exists.

In the region where no plug exists, the solution appears to be only very slightly yielded up to a certain value, after which it takes on a fully yielded profile. In fact, we will derive an asymptotic solution that has this property in Chapter 6. We call this type of solution a "pseudo plug solution" which is a term taken from Balmforth and Craster [2]. However, unlike the problem in [2], our solution can contain both regions where a real plug exists and regions with pseudo plug behavior. Other problems that exhibit pseudo plug behavior can be found in Mei & Yuhi [5], and Piau [6].

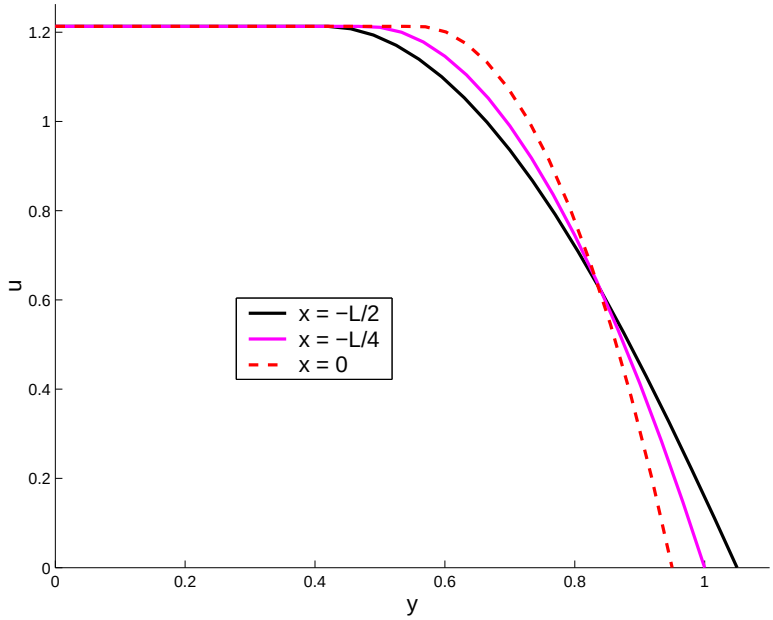

Figure 4.9: Cross-sections of the gap half-width. This is for $B = 5, h = .05, L = 4$, which yields the plug region shown in Fig. 4.5.

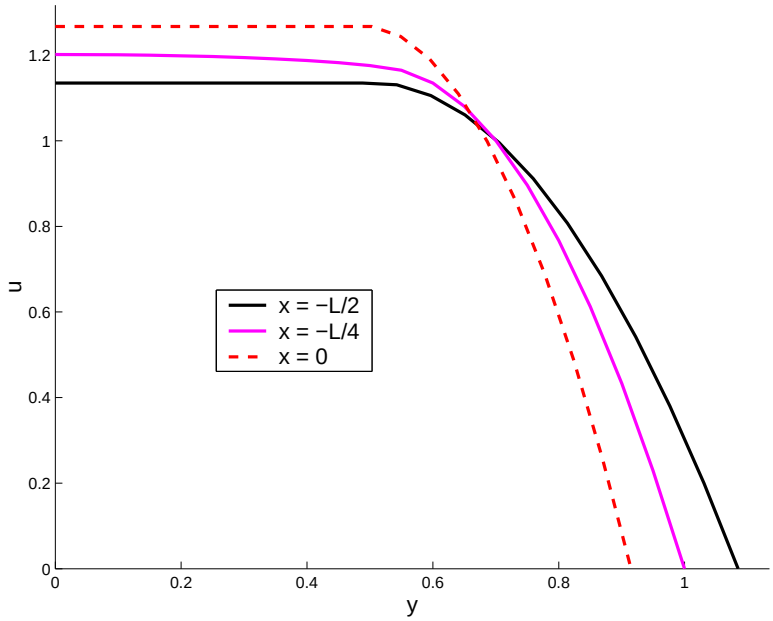

Figure 4.10: Cross-sections of the gap half-width. This is for $B = 5, h = .085, L = 20$, which yields the plug regions shown in Fig. 4.8.

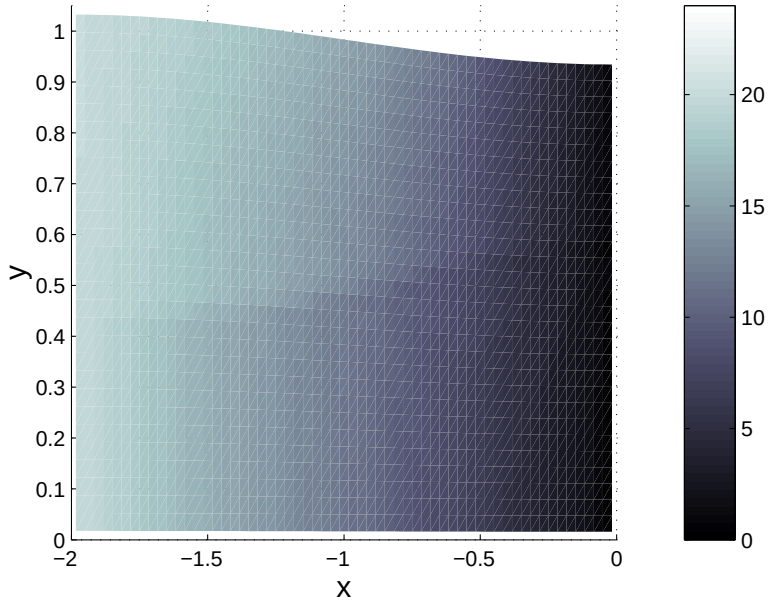

Figure 4.11: A colormap plot of the pressure field for $B = 5, h = .05, L = 4$.

Looking at Fig. 4.11, we see there is little change in pressure in the y direction. However, when looking closely, there is a small pressure change right on the interface between the plug region and the yielded flow (the plug region is show in Fig. 4.5).

Chapter 5
Asymptotic Solution

Is this chapter, we use the lubrication rescaling of the Navier-Stokes equations presented in Chapter 2 to build an asymptotic solution. The purpose of this analysis is to present a consistent solution for the Bingham model, i.e. a solution that exhibits a rigid plug region.

Recall that the notation in this section for velocity is $\mathbf{u} = \langle u, v \rangle$, which is not to be confused with the notation in Chapter 3.

5.1 Geometric Assumptions and Simplifications

For simplicity, it is assumed that the gap is symmetric about $y = 0$. This means that we can restrict our attention to only the upper half of the gap, $y \geq 0$. By assuming the gap is symmetric about $y = 0$, we are given by symmetry that $\tau_{xy} = 0$ and $v = 0$ on this line.

Also for simplicity, we take a sinusoidal variation of the gap half-width, i.e. $y_i(x) = 1 - h\cos(2\pi x)$. This assumption allows easy control over both the size of the variation, and the size of its derivative through a single parameter, h. However, we shall see that this analysis would remain true for any smooth wall variation with the size of both its amplitude and slope bounded by h. We will consider only one period of the channel in x.

In this analysis we assume a slow, steady flow and a small h. This means that we have $Re \sim \mathcal{O}(\delta)$ and both the amplitude and slope of the wall variation are $\mathcal{O}(\delta)$ as well. As we shall see, this causes the inertial terms in the momentum equations to be no larger than $\mathcal{O}(\delta^3)$ and since we only use terms up to $\mathcal{O}(\delta^2)$, they will not play a role in this analysis. The assumption of slow

flow is also essential to our method developed to determine the speed of the rigid plug which uses a result concerning slow visco-plastic flow presented by Prager [7].

5.2 Lubrication Rescalings

Recall from Chapter 2, that if we scale $\hat{x}$ with $\hat{L}$, $\hat{y}$ with $\hat{D}$, and introduce the small parameter $\delta \equiv \dfrac{\hat{D}}{\hat{L}}$, then the Navier-Stokes equations for steady flow become

$$\delta Re(u\frac{\partial u}{\partial x} + v\frac{\partial u}{\partial y}) = -\frac{\partial p}{\partial x} + \delta^2\frac{\partial}{\partial x}\tau_{xx} + \frac{\partial}{\partial y}\tau_{xy}, \tag{5.1}$$

$$\delta^3 Re(u\frac{\partial v}{\partial x} + v\frac{\partial v}{\partial y}) = -\frac{\partial p}{\partial y} + \delta^2\frac{\partial}{\partial x}\tau_{xy} + \delta^2\frac{\partial}{\partial y}\tau_{yy}, \tag{5.2}$$

$$\frac{\partial u}{\partial x} + \frac{\partial v}{\partial y} = 0. \tag{5.3}$$

Using the same rescaling on the constitutive laws for the Bingham fluid yields the following reduced constitutive laws:

$$\dot{\gamma}_{xy} = \frac{\partial u}{\partial y} + \delta^2\frac{\partial v}{\partial x}, \tag{5.4}$$

$$\dot{\gamma}_{xx} = 2\frac{\partial u}{\partial x}, \tag{5.5}$$

$$\dot{\gamma}_{yy} = 2\frac{\partial v}{\partial y}, \tag{5.6}$$

$$\dot{\gamma} = (\dot{\gamma}_{xy}^2 + \delta^2\dot{\gamma}_{xx}^2)^{\frac{1}{2}}. \tag{5.7}$$

The relation between the deviatoric stress and the rate-of-strain is now:

$$\tau_{ij} = \left(1 + \frac{B}{\dot{\gamma}}\right)\dot{\gamma}_{ij} \iff \tau > B, \tag{5.8}$$

$$\dot{\gamma} = 0 \iff \tau \leq B, \tag{5.9}$$

where B is the Bingham number given by

$$B = \frac{\tau_y \hat{D}}{\hat{\mu}\hat{U}_0} \tag{5.10}$$

and

$$\tau = (\tau_{xy}^2 + \delta^2\tau_{xx}^2)^{\frac{1}{2}}. \tag{5.11}$$

We now will construct an asymptotic solution for this flow, under the assumption of a small δ. First we will construct a solution for the yielded region. Then we will attempt to match this expansion to the plug solution. Lastly we will consider the problem of how to determine the speed of the plug (which is not given by the initial analysis).

5.3 Regular Expansion for the Yielded Region

We begin our general analysis of the flow described by the lubrication scaling by constructing an outer expansion in the fully yielded region. We take regular expansions in δ for u, v and p:

$$\begin{aligned} p &= p_0 + \delta p_1 + \delta^2 p_2 + \dots , \\ u &= u_0 + \delta u_1 + \delta^2 u_2 + \dots , \\ v &= v_0 + \delta v_1 + \delta^2 v_2 + \dots . \end{aligned}$$

For ease of notation, partial derivatives will now be written as a subscript x or y. The subscripts from expansion indices and subscripts from partial derivatives will be separated by a comma. Putting these regular expansions into the equations for the rate-of-strain, (5.4) - (5.7), gives the following expansions in δ:

$$\dot{\gamma}_{xy} = u_{0,y} + \delta u_{1,y} + \delta^2 (u_{2,y} + v_{0,x}) + \mathcal{O}(\delta^3), \tag{5.12}$$

$$\dot{\gamma}_{xx} = 2u_{0,x} + \delta 2u_{1,x} + \delta^2 2u_{2,x} + \mathcal{O}(\delta^3). \tag{5.13}$$

$$\dot{\gamma}^2 = u_{0,y}^2 + \delta 2u_{0,y}u_{1,y} + \delta^2 [2u_{0,y}(u_{2,y} + v_{0,x}) + u_{1,y}^2 + 4u_{0,x}^2] + \mathcal{O}(\delta^3) \tag{5.14}$$

Taking the square root of both sides, we find

$$\dot{\gamma} = |u_{0,y}| \left(1 + \delta \frac{2u_{1,y}}{u_{0,y}} + \delta^2 \frac{[2u_{0,y}(u_{2,y} + v_{0,x}) + u_{1,y}^2 + 4u_{0,x}^2]}{u_{0,y}^2} + \mathcal{O}(\delta^3) \right)^{\frac{1}{2}}. \tag{5.15}$$

Now we use a Taylor expansion in δ to get an expansion for $\dot{\gamma}^{-1}$,

$$\begin{aligned} \dot{\gamma}^{-1} &= \frac{1}{|u_{0,y}|} \left(1 - \delta \frac{u_{1,y}}{u_{0,y}} - \delta^2 \left[\frac{u_{2,y} + v_{0,x}}{u_{0,y}} + \frac{u_{1,y}^2}{2u_{0,y}^2} + \frac{2u_{0,x}^2}{u_{0,y}^2} \right] + \delta^2 \frac{3u_{1,y}^2}{2u_{0,y}^2} + \mathcal{O}(\delta^3) \right), \\ &= \frac{1}{|u_{0,y}|} \left(1 - \delta \frac{u_{1,y}}{u_{0,y}} - \delta^2 \frac{u_{0,y}(u_{2,y} + v_{0,x}) + 2u_{0,x}^2 - u_{1,y}^2}{u_{0,y}^2} + \mathcal{O}(\delta^3) \right). \end{aligned} \tag{5.16}$$

Using our expressions for the rate-of-strain and (5.8), we now find an expansion for the shear stress,

$$\begin{aligned}\tau_{xy} &= \{u_{0,y} + B\text{sign}(u_{0,y}) + \delta u_{1,y} \\ &\quad + \delta^2 \left[u_{2,y} + v_{0,x} - B\text{sign}(u_{0,y}) \frac{2u_{0,x}^2}{u_{0,y}^2} \right] + \mathcal{O}(\delta^3) \Bigg\} \\ &\equiv \tau_{xy,0} + \delta\tau_{xy,1} + \delta^2\tau_{xy,2} + \mathcal{O}(\delta^3). \end{aligned} \tag{5.17}$$

For $\tau_{xx} = -\tau_{yy}$ we shall only need the leading order term,

$$\tau_{xx} = 2\left(1 + \frac{B}{|u_{0,y}|}\right) u_{0,x} + \mathcal{O}(\delta). \tag{5.18}$$

Substitute the expansions for u, v, p, and τ_{ij} into the Momentum Equations,(5.1) and (5.2), and balance orders of δ to get the zeroth, first and second order problems. Recall that we have $Re \sim \mathcal{O}(\delta)$ because we have assumed a slow flow.

$$\mathcal{O}(1): \quad 0 = -p_{0,x} + u_{0,yy}, \tag{5.19}$$

$$0 = p_{0,y}. \tag{5.20}$$

$$\mathcal{O}(\delta): \quad 0 = -p_{1,x} + u_{1,yy}, \tag{5.21}$$

$$0 = p_{1,y}. \tag{5.22}$$

$$\mathcal{O}(\delta^2): \quad 0 = -u_0 u_{0,x} - v_0 u_{0,y} - p_{2,x} + \frac{\partial}{\partial y}\tau_{xy,2} + \frac{\partial}{\partial x}\tau_{xx,0}\ , \tag{5.23}$$

$$0 = -p_{2,y} + \frac{\partial}{\partial x}\tau_{xy,0} + \frac{\partial}{\partial y}\tau_{yy,0}. \tag{5.24}$$

Recall we have the channel half-width being $y_i(x) = 1 - h\cos(2\pi x)$ and we have assumed $h \sim \mathcal{O}(\delta)$. We shall see in the following section that $u_0 = u_0(y_i(x), y)$ and therefore if $h \sim \mathcal{O}(\delta)$, we have that $u_x \sim \mathcal{O}(\delta)$ and by integrating the incompressibility condition out from $y = 0$ we get $v_0 = 0$. This means the inertial terms in (5.23) should actually be in the $\mathcal{O}(\delta^3)$ problem.

We also get as a result of $h \sim \mathcal{O}(\delta)$:

$$\begin{aligned} \frac{\partial}{\partial x}\tau_{xy,0} &\sim \mathcal{O}(\delta), \\ \tau_{xx,0} &= 0, \\ \tau_{yy,0} &= 0, \\ \tau_{xy,2} &= u_{2,y}. \end{aligned}$$

Therefore, from the assumption of $h \sim \mathcal{O}(\delta)$, we get the following problem at second order:

$$\mathcal{O}(\delta^2): \quad 0 = -p_{2,x} + u_{2,yy}, \tag{5.25}$$

$$0 = p_{2,y}. \tag{5.26}$$

5.4 The Zeroth Order Solution

The leading order equations give:

$$p_{0,y} = 0 \Longrightarrow p_0 = p_0(x), \tag{5.27}$$

$$\begin{aligned} p_{0,x} = \frac{\partial}{\partial y}(u_{0,y} + \text{sign}(u_{0,y})B) &\iff \tau > B, \\ u_{0,y} = 0 &\iff \tau \leq B. \end{aligned} \tag{5.28}$$

To leading order, $\tau_0 = |\tau_{xy,0}|$. The continuity equation at leading order is

$$u_{0,x} + v_{0,y} = 0. \tag{5.29}$$

The leading order solution should also satisfy the imposed flow constraint, i.e.

$$\int_0^{y_i(x)} u_0 \, dy = 1 \quad \forall x. \tag{5.30}$$

In the region where $\tau > B$, we have at leading order

$$p_{0,x} = \frac{\partial}{\partial y}\tau_{xy,0}. \tag{5.31}$$

Remembering that there is no shear stress on $y = 0$ and, $p_0 = p_0(x)$, we integrate (5.31) with respect to y out from the centerline to get

$$p_{0,x}y = u_{0,y} + \text{sign}(u_{0,y})B. \tag{5.32}$$

So, for $\tau > B$,

$$u_{0,y} = p_{0,x}y - \text{sign}(u_{0,y})B. \tag{5.33}$$

Now, when $\tau = B$ there is a yield surface, call it y_y. In the unyielded region, $u_{0,y} = 0$, so for continuity of derivatives, and hence continuity of shear stress, we need $u_{0,y} \to 0$ as $y \to y_y$ from the yielded region. Using this in (5.33) tells us about the position of the yield surface. (Note: This "yield surface" is only the leading order yield surface, and the actual yield surface may be different, or may not exist at all.)

$$y_y = \text{sign}(u_{0,y})\frac{B}{p_{0,x}}. \tag{5.34}$$

But, we know $0 \leq y_y \leq y_i$, so,

$$y_y = \frac{B}{|p_{0,x}|}, \tag{5.35}$$

where $\tau(y_y)_0 = B$, and $\text{sign}(u_{0,y}) = \text{sign}(p_{0,x})$. This means (5.33) can be written as

$$u_{0,y} = p_{0,x}(y - y_y). \tag{5.36}$$

Recalling that $u(y_i) = 0$, we again integrate with respect to y, this time in from y_i.

$$\int_{y_i}^{y} u_{0,y}\, dy = \int_{y_i}^{y} p_{0,x}(y - y_y)\, dy, \tag{5.37}$$

so,

$$u_0(y_i(x), y) = p_{0,x}\left[\frac{(y - y_y)^2}{2} - \frac{(y_i - y_y)^2}{2}\right]. \tag{5.38}$$

We have imposed a pressure drop to cause a flow in the positive u direction, i.e. $u_0 \geq 0$. This means our leading order velocity is

$$u_0(y_i, y) = \frac{|p_{0,x}|}{2}\left[(y_i - y_y)^2 - (y - y_y)^2\right]. \tag{5.39}$$

Now, recall

$$\tau = (\tau_{xy,0}^2 + \mathcal{O}(\delta))^{\frac{1}{2}} = y|p_{0,x}|(1 + \mathcal{O}(\delta))^{\frac{1}{2}}. \tag{5.40}$$

Clearly τ is monotonically increasing with y. This means τ is largest near the wall, and $\tau > B$ on $y \in (y_y, y_i]$. This means

$$u_0 = \frac{B}{2y_y}[(y_i - y_y]^2 - (y - y_y)^2] \,, \quad y \in (y_y, y_i]. \tag{5.41}$$

For the unyielded region, we have u constant. For continuity of u at y_y, we need

$$u_0 = \frac{B}{2y_y}(y_i - y_y)^2 \,, \quad y \in [0, y_y]. \tag{5.42}$$

Note, according to (5.35), at leading order, there is always a plug region. However, if $y_y \geq y_i$, then the pressure drop is not enough to force movement and $u_0 \equiv 0$.

Now, we use the imposed flow rate across the gap, (5.30), and the expressions for u_0, (5.41), and (5.42) to get

$$\frac{B}{2}(y_i - y_y)^2 + \int_{y_y}^{y_i} \frac{B}{2y_y}[(y_i - y_y)^2 - (y - y_y)^2]\, dy \; = 1. \tag{5.43}$$

Integrating, expanding terms, and multiplying both sides by y_y gives

$$\frac{B}{6}y_y^3 - (\frac{By_i^2}{2} + 1)y_y + \frac{By_i^3}{3} = 0. \tag{5.44}$$

If we let

$$y_y = \frac{y_i}{\xi}, \tag{5.45}$$

then

$$\frac{By_i^3}{3}\xi^3 - (\frac{By_i^3}{2} + y_i)\xi^2 + \frac{By_i^3}{6} = 0. \tag{5.46}$$

Divide (5.46) by $\dfrac{By_i^3}{6}$ and let $\widetilde{B} = By_i^2$ to get

$$2\xi^3 - (3 + \frac{6}{\widetilde{B}})\xi^2 + 1 = 0. \tag{5.47}$$

Call the above polynomial $P(\xi)$ and remember that $\widetilde{B} > 0$. Note that,

$$\begin{aligned} P(-\infty) \; &< 0 < \; P(0), \\ P(0) \; &> 0 > \; P(1), \\ P(1) \; &< 0 < \; P(\infty). \end{aligned}$$

This means that there is exactly one zero of $P(\xi)$ in each of the intervals: $(-\infty, 0)$, $(0, 1)$, and $(1, \infty)$. Now, $0 < y_y < y_i$ which means that $\xi > 1$, leaving exactly one choice for $\xi_{root} = \xi(\widetilde{B})$.

5.4.1 Zeroth Order Results

The root $\xi_{root}(\widetilde{B})$ is easy to find numerically using e.g. bisection. In Fig. (5.1) we plot y_y and y_i vs. x for various values B. The same is done in Fig. (5.2), but with an increased value of h.

We note that with a fixed B, for each x we will have a different value of $\widetilde{B}$ and hence a different $y_y(x)$. It is $y_y(x)$ that characterizes u_0, through (5.41), (5.42) and defines $p_{0,x}$ through (5.35). It is easy to see from Fig. 5.1 that y_y closely follows the shape of y_i. It is difficult to tell from these pictures, but in fact, the value $y_i(x) - y_y(x)$ is **not** constant in x. As B increases, y_y shifts closer to the mud interface. Furthermore, from our plots of $|p_{0,x}|$ in Fig. 5.1 we can see that for higher Bingham numbers, a larger pressure drop is needed to drive the flow. Also, we notice that $|p_{0,x}|$ is larger at the narrower parts of the channel.

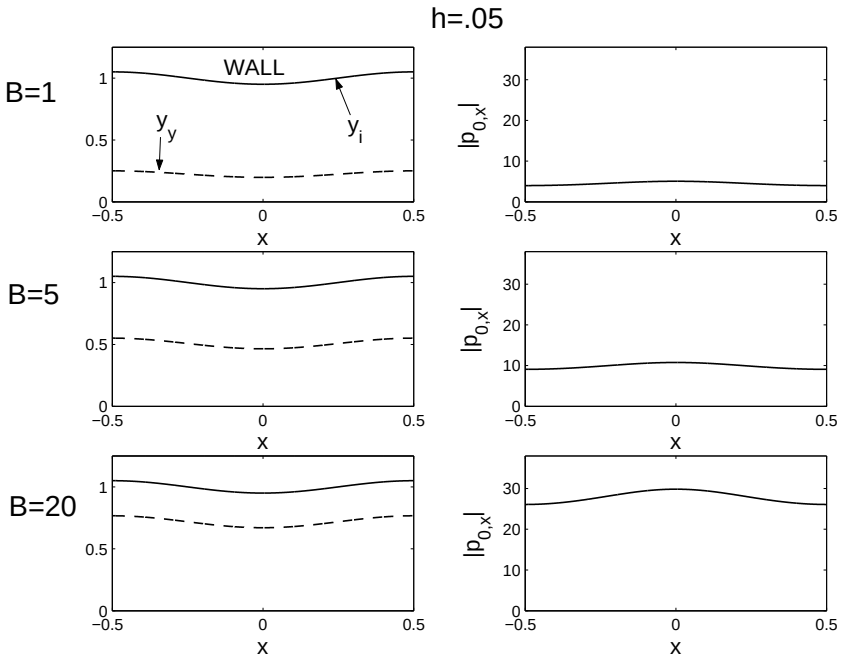

Figure 5.1: Plots of y_y and $|p_{0,x}|$ for $B = 1, 5$ and 20 with $h = .05$.

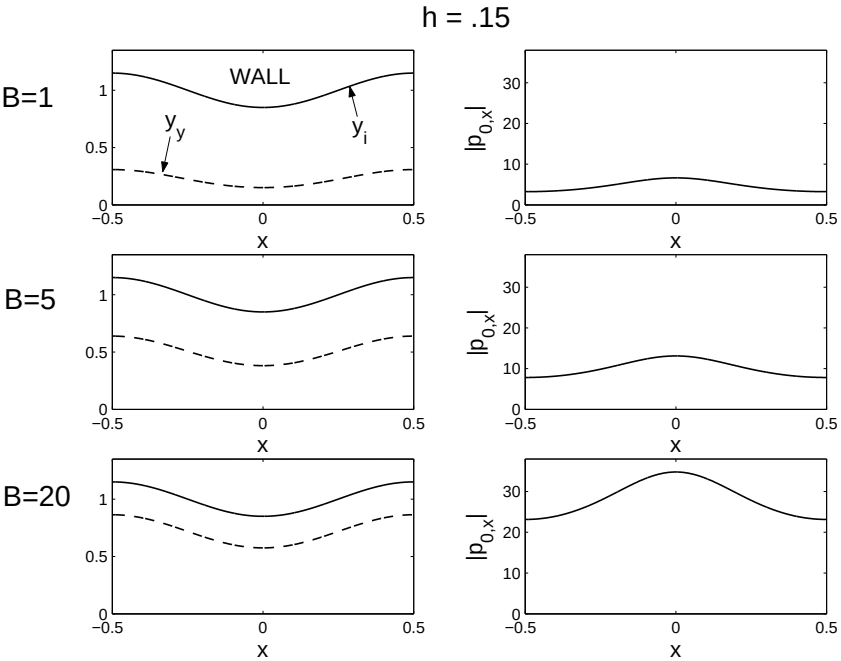

Figure 5.2: Plots of y_y and $|p_{0,x}|$ for $B = 1, 5$ and 20 with $h = .15$.

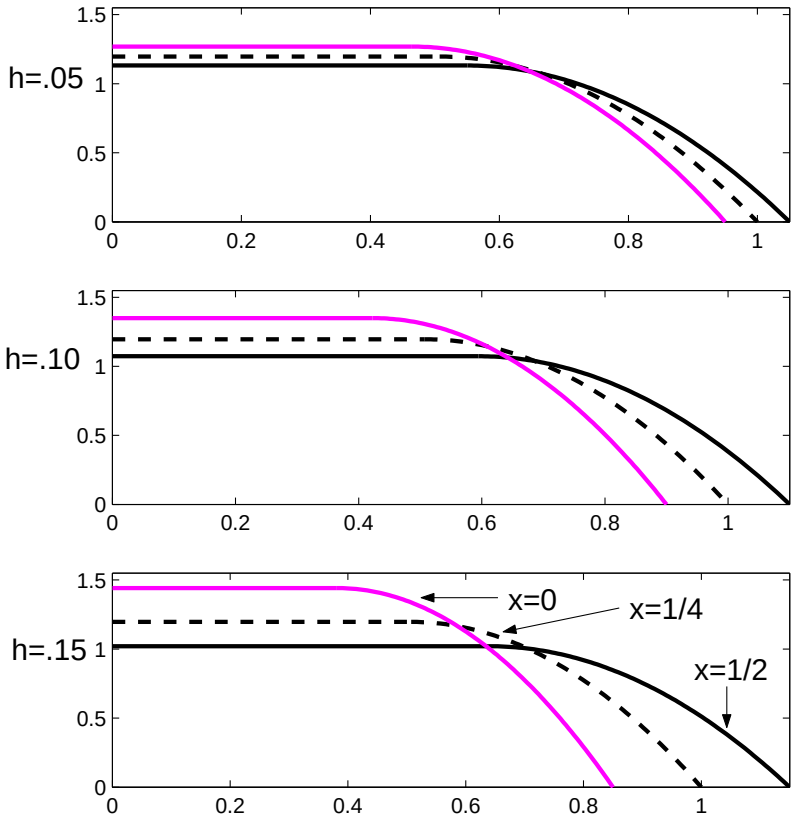

Figure 5.3: Plots of $u_0(0,y), u_0(\frac{1}{4},y)$ and $u_0(\frac{1}{2},y)$ for various amplitudes of $y_i(x)$. $B = 5$ was used in all 3 plots.

To examine u_0, we look at plots of $u_0(y)$ for $x = 0, \frac{1}{4}$ and $\frac{1}{2}$ superimposed on the same axes in Fig. 5.3. Note that u_0 has different "plug speeds" for different $y_i(x)$. Hence if $y_i'(x) \neq 0$, then $u_{0,x} \neq 0$ for $y < y_y$, and therefore u_0 does not have real plug regions at all. For larger h we see that the difference in "plug speeds" is greater over the length of the gap. This leading order inconsistency arising from the lubrication scaling has been known and studied for some time now. See [1], [2], [6] and [5] for some discussions. For the remainder of this paper,we will use the notation

$$u_0(y_y) \equiv u^{pp}(x).$$

This notation emphasizes the fact that the "plug speed" in the zeroth order solution varies in x. The "pp" superscript stands for "pseudo plug".

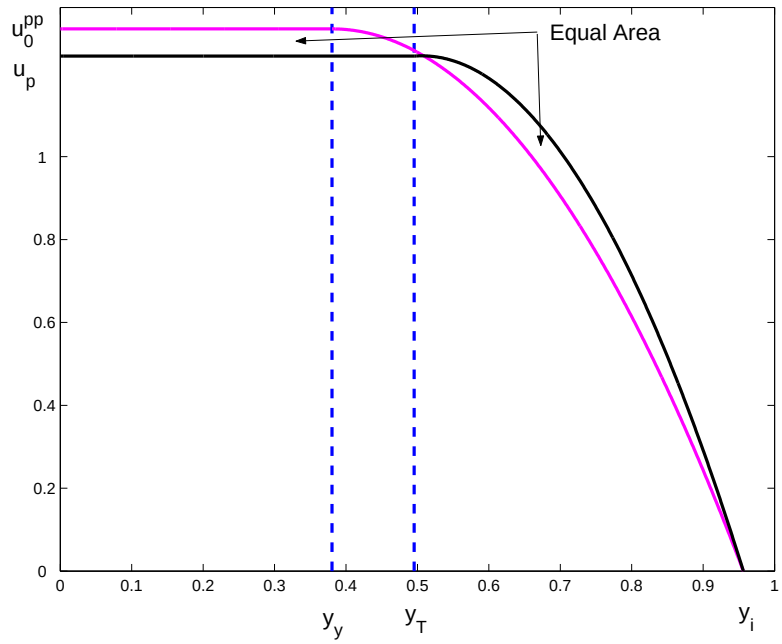

Figure 5.4: This is an example of a plot of u_0 and the asymptotically corrected solution for an instance when $u_p < u_0^{pp}$. This figure illustrates why we must have $y_y < y_T$ when $u_p < u_0^{pp}$ in order to maintain a unit flow rate across the half-gap width.

In our problem we know that if the amplitude of the sinusoidal wall variation, h, is small enough, there will be an intact plug for the entire length of the slot. This plug will have some uniform velocity $u = u_p$, yet to be determined. In order to capture this behavior, we will assume that there is a real yield surface, y_T, inside of which $\mathbf{u} = \langle u_p, 0 \rangle$. We will then construct $\mathcal{O}(\delta)$ and $\mathcal{O}(\delta^2)$ corrections to the outer solution that connect to the true plug.

For any given x, the outer solution has a "pseudo-plug" speed of $u_0(y_y) \equiv u^{pp}(x)$. If $u^{pp}(x) < u_p$, then to preserve a flow-rate of 1, would require $y_T < y_y$. However, to have $u^{pp} > u_p$ would require $y_T > y_y$. If $u^{pp} = u_p$, then we will have $u = u_0$. See Fig. (5.4) to get a visual demonstration of this.

Note that although u_p is constant, it has not yet been determined. This is dealt with in §5.8. Without knowing u_p, we can assume that it is in the range:

$$\left[\frac{B}{2y_y}(y_i - y_y)^2\right]_{x=-\frac{1}{2}} \leq u_p \leq \left[\frac{B}{2y_y}(y_i - y_y)^2\right]_{x=0} , \tag{5.48}$$

since these are the plug velocities of the outer solution.

We will treat the cases $y_T < y_y$ and $y_T > y_y$ separately as they will require slightly different solutions. For the case $y_T < y_y$, we will have an inner transition layer of thickness δ connecting the plug to the fully plastic region. For the case $y_T > y_y$, we will match the plug and the plastic region at a single point, y_T.

Later, in §6.1 we will construct a solution for the case when the wall amplitude is large enough to make the plug actually break. The criteria for judging when the plug will actually break is derived in §6.2.

5.5 Corrected Solution for $y_T < y_y$

In this section we assume that we are in a part of the channel with $u^{pp} < u_p$ and hence $y_T < y_y$. The velocity profile will have the form:

$$u = u_p \quad \text{for } y \in [0, y_T] \ , \tag{5.49}$$

$$u = u_p + \delta^2 u_2^i(x,y) + \dots \quad \text{for } y \in (y_T, y_y) \ , \tag{5.50}$$

$$u = u^{pp}(x) + \delta u_1(x,y) + \delta^2 u_2(x,y) + \dots \quad \text{for } y \in [y_y, y_i] \ , \tag{5.51}$$

and we shall see $y_y - y_T \sim \mathcal{O}(\delta)$. We will begin by constructing u_1 and u_2. In the next section, we will construct the inner solution, u_2^i, and match the three layers. Only after that will the case $y_T > y_y$ will be treated.

The $\mathcal{O}(\delta)$ problem in the yielded region is:

$$u_{1,yy} - p_{1,x} = 0, \tag{5.52}$$

$$p_{1,y} = 0, \tag{5.53}$$

$$u_{1,x} + v_{1,y} = 0, \tag{5.54}$$

$$u_1(y_i) = v_1(y_i) = 0. \tag{5.55}$$

We make the following definitions:

$$u_1(y_y) \equiv u_1^*, \tag{5.56}$$

$$\int_{y_y}^{y_i} u_1 \equiv q_1, \tag{5.57}$$

and note that for given u_1^* and q_1, we can solve for u_1 and $p_{1,x}$ by integrating (5.52) with respect to y. We find that:

$$u_1 = p_{1,x}\frac{(y-y_y)(y-y_i)}{2} + u_1^*\left(\frac{y-y_i}{y_y-y_i}\right), \tag{5.58}$$

$$\int_{y_y}^{y_i} u_1 = -\frac{1}{12}(y_i-y_y)^3 p_{1,x} + u_1^*\frac{y_i-y_y}{2} = q_1, \tag{5.59}$$

and

$$p_{1,x} = -\frac{12q_1}{(y_i-y_y)^3} + \frac{6u_1^*}{(y_i-y_y)^2}. \tag{5.60}$$

Substituting (5.60) into (5.58) gives the following formula for u_1 depending on u_1^* and q_1 only:

$$u_1 = \frac{(y-y_i)}{(y_i-y_y)^2}\left[u_1^*(3y-2y_y-y_i) - 6q_1\frac{(y-y_y)}{(y_i-y_y)}\right]. \tag{5.61}$$

The values u_1^* and q_1 will be found in the next section by matching u_1 to an inner expansion in a transition layer between the plug and and the fully yielded flow.

Under the assumption that $h \sim \mathcal{O}(\delta)$, the $\mathcal{O}(\delta^2)$ problem looks exactly like the $\mathcal{O}(\delta)$ problem. Therefore, we have

$$u_2 = \frac{(y-y_i)}{(y_i-y_y)^2}\left[u_2^*(3y-2y_y-y_i) - 6q_2\frac{(y-y_y)}{(y_i-y_y)}\right]. \tag{5.62}$$

Again, u_2^* and q_2 are defined by

$$u_2(y_y) \equiv u_2^*, \tag{5.63}$$

$$\int_{y_y}^{y_i} u_2 \equiv q_2. \tag{5.64}$$

5.5.1 Solution in the Transition Layer for $y_T < y_y$

In the transition layer, we take the expansion

$$u^i = u_p + \delta^2 u_2^i(x,y) + \delta^3 u_3^i(x,y) + \dots \quad . \tag{5.65}$$

As we will see, this will result in a layer where $\dot{\gamma} \sim \mathcal{O}(\delta)$ and $\tau_{xy} = B + \mathcal{O}(\delta)$. This layer has thickness $\mathcal{O}(\delta)$ so we rescale y like

$$y = y_T(x) + \delta\xi, \tag{5.66}$$

and we define

$$\xi_T(x) \equiv \frac{y_y(x) - y_T(x)}{\delta}. \tag{5.67}$$

With this expansion for u, we can find the size of v through integrating the continuity equation out from the true yield surface.

$$v^i = \int_{y_T}^{y} u^i_x dy \sim \int_{y_T}^{y} \delta^2 u^i_{2,x} \sim \mathcal{O}(\delta^3). \tag{5.68}$$

We find that $v^i \sim \mathcal{O}(\delta^3)$ because $v = 0$ in the plug and we have only integrated over an interval of size δ. This makes v^i such small magnitude that it can be neglected in the expansions for rate-of-strain and hence does not play a role in the transition layer.

Taking our expansion for u^i and our knowledge that $v^i \sim \mathcal{O}(\delta^3)$, we get the following expressions for our rate-of-strain components:

$$\dot{\gamma}_{xy} = \delta u^i_{2,\xi} + \delta^2 u^i_{3,\xi} + \dots \quad , \tag{5.69}$$

$$\dot{\gamma}_{xx} = \delta^2 2u^i_{2,x} + \dots \quad , \tag{5.70}$$

$$\dot{\gamma}^2 = \delta^2 (u^i_{2,\xi})^2 + \delta^3 2u^i_{2,\xi} u^i_{3,\xi} + \dots \quad , \tag{5.71}$$

$$\dot{\gamma}^{-1} = \frac{1}{\delta |u^i_{2,\xi}|} \left(1 - \delta \frac{u^i_{3,\xi}}{u^i_{2,\xi}} + \mathcal{O}(\delta^2) \right). \tag{5.72}$$

We now use equation (5.72) to get an expansion for the shear stress in the inner region.

$$\begin{aligned} \tau_{xy} &= \left[1 + \frac{B}{\delta |u^i_{2,\xi}|} \left(1 - \delta \frac{u^i_{3,\xi}}{u^i_{2,\xi}} + \mathcal{O}(\delta^2) \right) \right] \delta u^i_{2,\xi} \left[1 + \delta \frac{u^i_{3,\xi}}{u^i_{2,\xi}} + \mathcal{O}(\delta^2) \right] \\ &= B \ \mathrm{sign}(u^i_{2,\xi}) + \delta u^i_{2,\xi} + \mathcal{O}(\delta^2). \end{aligned} \tag{5.73}$$

The leading order equations for the transition layer are now:

$$0 = -p_{0,x} + \frac{\partial}{\partial \xi} u^i_{2,\xi}, \tag{5.74}$$

$$0 = p_{0,\xi}, \tag{5.75}$$

$$0 = u^i_2(y_T) = u^i_{2,y}(y_T). \tag{5.76}$$

Because p_0 does not depend on ξ, integrating equation (5.74) from $\xi = 0$ out into the transition layer twice and applying the boundary conditions (5.76) gives the following expression for u_2^i:

$$u_2^i = p_{0,x}\frac{\xi^2}{2} = -\frac{B}{2y_y}\xi^2 < 0. \tag{5.77}$$

5.5.2 Matching for $y_T < y_y$

In this section, we will determine q_1, q_2, u_1^*, u_2^* and y_T for the case $y_T < y_y$. This will lead to a description of the solution that depends only on the remaining unknown quantity u_p. A method for determining u_p is presented in §5.8.

To avoid confusion in notation, the outer solution in the plastic region is denoted with a superscript o, e.g. u^o, and the inner solution with a superscript i, e.g. u^i.

The overall aim now is to match the velocity and stress at each order, within the inner layer. At the same time, we must ensure that $\int_0^{y_i} u\, dy = 1$.

Recall from the previous section that at y_y we have, in terms of the inner variables:

$$u^i(y_y) = u_p - \delta^2\frac{B}{2y_y}\xi_T^2 + \mathcal{O}(\delta^3), \tag{5.78}$$

$$\tau_{xy}^i(y_y) = -B - \delta\frac{B}{y_y}\xi_T + \mathcal{O}(\delta^2). \tag{5.79}$$

Recall from our outer solution that at y_y we have

$$u^o(y_y) = u^{pp}(x) + \delta u_1^* + \delta^2 u_2^* + \mathcal{O}(\delta^3), \tag{5.80}$$

$$\tau_{xy}^o(y_y) = -B + \delta u_{1,y}^o(y_y) + \delta^2 u_{2,y}^o(y_y) + \mathcal{O}(\delta^3). \tag{5.81}$$

Continuity of Velocity when $y_T < y_y$

It is evident that for $h \neq 0$ we have $u^p p(x) \neq u_p$. However, if $h \sim \mathcal{O}(\delta)$, then the total variation in $u^{pp}(x)$ is also $\mathcal{O}(\delta)$. To see this we could take a perturbation expansion of the solution $\xi_{root}(\widetilde{B})$ about the value $\xi_{root}(B)$, i.e. for $y_i = 1$. Therefore, we have that $u_p - u^{pp}(x) \sim \mathcal{O}(\delta)$, provided that equation (5.48) holds. In the inner layer, $u^i \sim u_p + \mathcal{O}(\delta^2)$, so we must match the discrepancy between u_p and $u_0^o(y_y)$ with u_1^*, so

$$u_1* = \frac{1}{\delta}\left[u_p - u^{pp}(x)\right]. \tag{5.82}$$

Then to match the $\mathcal{O}(\delta^2)$ terms in (5.78) and (5.80) we must have

$$u_2^* = -\frac{B}{2y_y}\xi_T^2. \tag{5.83}$$

Finding q_1 and q_2 when $y_T < y_y$

To find q_1 and q_2 we consider the total flow across the channel. For the outer solution, u^o, we have

$$\begin{aligned}\int_{y_y}^{y_i} u^o &= \int_{y_y}^{y_i} u_0^o + \delta u_1^o + \delta^2 u_2^o \, dy \\ &= 1 - y_y u^{pp}(x) + \delta q_1 + \delta^2 q_2 + \mathcal{O}(\delta^3).\end{aligned} \tag{5.84}$$

We also know

$$\int_0^{y_y} u \, dy = \int_0^{y_T} u_p \, dy + \int_{y_T}^{y_y} u_p + \delta^2 u_2^i \, dy = y_y u_p + \mathcal{O}(\delta^3), \tag{5.85}$$

since $y_y - y_T \sim \mathcal{O}(\delta)$.

Combining this with the fact that the total flow across the gap half-width is 1, we have

$$0 = y_y \left[u_p - u^{pp}(x)\right] + \delta q_1 + \delta^2 q_2 + \mathcal{O}(\delta^3). \tag{5.86}$$

We now recognize the expression in brackets as δu_1^* and rewrite the equation as

$$0 = \delta(y_y u_1^* + q_1) + \delta^2 q_2. \tag{5.87}$$

Matching orders gives

$$q_1 = -y_y u_1^*, \tag{5.88}$$

$$q_2 = 0. \tag{5.89}$$

Matching the Shear Stress for $y_T < y_y$

In order to match $\tau_{xy}^o(y_y)$ from (5.81) with $\tau_{xy}^i(y_y)$ from (5.79), we need to know $u_{1,y}^o$. We can find an explicit expression for $u_{1,y}^o$ by differentiating equation (5.61), and using the fact that $q_1 = -y_y u_1^*$.

$$u_{1,y}^o(y) = \frac{1}{(y_i - y_y)^2}\left[u_1^*(3y - 2y_y - y_i) + 3u_1^*(y - y_i) + 6y_y u_1^* \frac{(2y - y_y - y_i)}{(y_i - y_y)}\right],$$

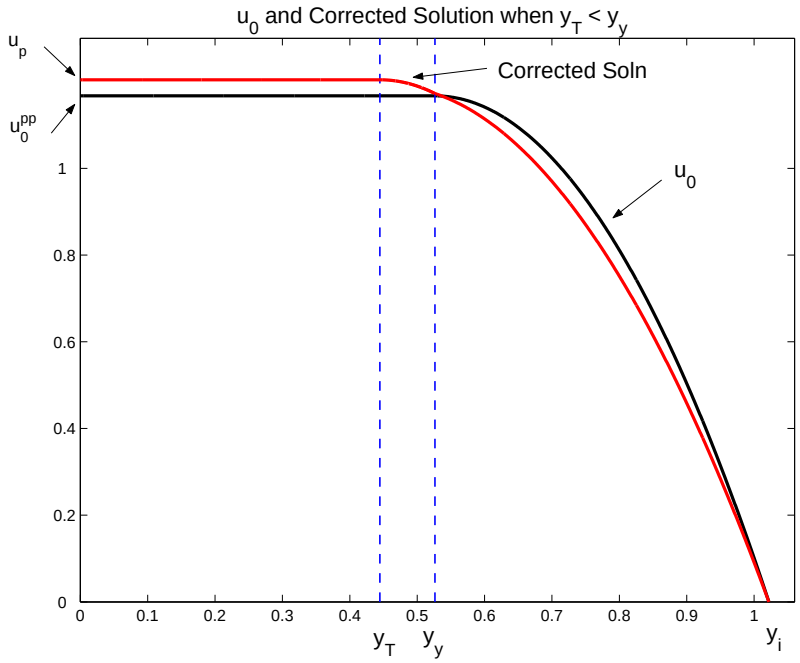

Figure 5.5: A plot of u_0 and u corrected to $\mathcal{O}(\delta^2)$ on a cross-section of the channel half-width where $y_T < y_y$. The parameters used were $B = 5$, $h = .04$, $\delta = .05$. The plug speed was determined by the method presented in §5.8.

$$u^o_{1,y}(y_y) = \frac{-2u^*_1}{(y_i - y_y)^2}(y_y + 2y_i). \tag{5.90}$$

Substitute (5.90) into equation (5.81) and we have

$$\tau^o_{xy}(y_y) = -B - \delta\frac{2u^*_1}{(y_i - y_y)^2}(y_y + 2y_i) + \mathcal{O}(\delta^2). \tag{5.91}$$

For (5.81) and (5.91) to agree at $\mathcal{O}(\delta)$ we must have

$$\begin{aligned} \xi_T &= \frac{2y_y u^*_1}{B(y_i - y_y)^2}(y_y + 2y_i) \\ &= (y_y + 2y_i)\frac{u^*_1}{u^{pp}_0} \\ &= (y_y + 2y_i)\left[\frac{u_p}{u^{pp}_0} - 1\right]\frac{1}{\delta}. \end{aligned} \tag{5.92}$$

Notice that $\xi_T \sim \mathcal{O}(1)$ as required.

5.5.3 Composite Solution: $y_T < y_y$

The solution for $y_T < y_y$ is now complete and is given by:

$$\begin{aligned} y > y_y \quad & u \sim \quad u_0^o + \delta u_1^o + \delta^2 u_2^o, \\ y \in (y_T, y_y) \quad & u \sim \quad u_p + \delta^2 u_2^i, \\ y \in [0, y_T] \quad & u \sim \quad u_p, \end{aligned}$$

where

$$y_T = y_y - \delta\xi_T = y_y - (y_y + 2y_i)\left[\frac{u_p}{u_0^{pp}} - 1\right], \tag{5.93}$$

$$u_0^o = \frac{B}{2y_y}\left[(y_i - y_y)^2 - (y - y_y)^2\right], \tag{5.94}$$

$$u_1^o = u_1^* \frac{(y - y_i)}{(y_i - y_y)^2}\left[(3y - 2y_y - y_i) + 6y_y \frac{(y - y_y)}{(y_i - y_y)}\right], \tag{5.95}$$

$$u_2^o = u_2^* \frac{(y - y_i)}{(y_i - y_y)^2}(3y - 2y_y - y_i), \tag{5.96}$$

$$u_1^* = \frac{u_p - u_0^o(y_y)}{\delta}, \tag{5.97}$$

$$u_2^* = -\frac{B}{2y_y}\xi_T^2, \tag{5.98}$$

$$u_2^i = -\frac{B}{2y_y}\frac{(y - y_T)^2}{\delta^2}, \tag{5.99}$$

and

$$p_x = -\frac{B}{y_y} + \delta\frac{6u_1^*}{(y_i - y_y)^2}\left(\frac{2y_y}{(y_i - y_y)} + 1\right) + \delta^2\frac{6u_2^*}{(y_i - y_y)^2} + \mathcal{O}(\delta^3). \tag{5.100}$$

The only thing not yet determined is the actual plug speed, u_p, which will be found in §5.8. Fig. (5.5) shows a plot of u_0 and u corrected to $\mathcal{O}(\delta^2)$ vs. y on a cross-section taken in a part of the channel where $y_T < y_y$. To get the plug speed for this plot, the method presented in §5.8 was used.

5.6 Corrected Solution for $y_y < y_T$

To construct a solution when $u_p < u_o^0(y_y)$, we assume the following structure:

$$u = u_p \quad \text{for } y \in [0, y_T], \tag{5.101}$$

$$u = u_0(y_i, y) + \delta u_1(x, y) + \delta^2 u_2(x, y) \quad \text{for } y \in (y_T, y_i]. \tag{5.102}$$

We must choose u_1 and u_2 so that velocity and stress are continuous at the point y_T, and the unit flow-rate is maintained. This differs from our approach in the case $y_y > y_T$ where we had an inner transition layer, but the results will look very similar.

In order to have continuity of velocity at y_T we need

$$u_p = u_0(y_T) + \delta u_1(y_T) + \delta^2 u_2(y_T).$$

Recall, because $h \sim \mathcal{O}(\delta)$, we have $|u_p - u_0(y_y)| \sim \mathcal{O}(\delta)$. Furthermore, $|y_T - y_y| \sim \mathcal{O}(\delta)$ which implies that $|u_0(y_y) - u_0(y_T)| \sim \mathcal{O}(\delta^2)$. This suggests that we let $u_1(y_T)$ compensate for the $\mathcal{O}(\delta)$ difference between u_p and $u_0(y_y)$, and let $u_2(y_T)$ compensate for the $\mathcal{O}(\delta^2)$ change in u_0 over the interval (y_y, y_T), i.e.:

$$u_1(y_T) = \frac{1}{\delta}\left(u_p - u^{pp}(x)\right) \equiv u_1^*, \tag{5.103}$$

$$u_2(y_T) = \frac{1}{\delta^2}\left(u_0(y_y) - u_0(y_T)\right) \equiv u_2^*. \tag{5.104}$$

In order to maintain a unit flow-rate, we need

$$\int_0^{y_T} u_p + \int_{y_T}^{y_i} u_o + \delta u_1 + \delta^2 u_2 = 1. \tag{5.105}$$

However, we have already constructed u_0 in such a way that

$$\int_0^{y_y} u_0 + \int_{y_y}^{y_i} u_0 = 1. \tag{5.106}$$

Subtracting (5.106) from (5.105) we see

$$\int_0^{y_y} [u_p - u_0(y_y)] + \int_{y_y}^{y_T} [u_p - u_0(y)] + \delta \int_{y_T}^{y_i} u_1 + \delta^2 \int_{y_T}^{y_i} u_2 = 0. \tag{5.107}$$

Furthermore, we can use (5.103) to write the first term in (5.107) in terms of u_1^*. Doing this we get

$$\delta y_y u_1^* + \delta u_1^*(y_T - y_y) + \frac{B}{6y_y}(y_T - y_y)^3 + \int_{y_T}^{y_i} u_1 + \delta^2 \int_{y_T}^{y_i} u_2^* = 0. \tag{5.108}$$

Note the first two terms can be combined to make $\delta y_T u_1^*$. Balancing orders in (5.108) tells us about q_1 and q_2.

$$\int_{y_T}^{y_i} u_1 = \quad -y_T u_1^* \quad \equiv q_1, \tag{5.109}$$

$$\int_{y_T}^{y_i} u_2 = \qquad 0 \qquad \equiv q_2. \tag{5.110}$$

The $\mathcal{O}(\delta)$ problem presented at the beginning of §5.5 still applies here, except now $u_1^* \equiv u_1(y_T)$. The solution is now

$$u_1 = \frac{\partial p_1}{\partial x}\frac{(y - y_T)(y - y_i)}{2} + u_1^*\left(\frac{y - y_i}{y_T - y_i}\right). \tag{5.111}$$

The definition of q_1 has also been altered to use y_T instead of y_y in the lower limit of integration. Integrating the new expression for u_1 relates $p_{1,x}$ and q_1.

$$\int_{y_T}^{y_i} u_1 = -\frac{1}{12}(y_i - y_T)^3 p_{1,x} + u_1^*\frac{y_i - y_T}{2} = q_1. \tag{5.112}$$

Solving for $p_{1,x}$ gives an expression depending on y_T, u_1^* and q_1.

$$p_{1,x} = -\frac{12q_1}{(y_i - y_T)^3} + \frac{6u_1^*}{(y_i - y_T)^2}. \tag{5.113}$$

Substituting (5.113) into (5.111) and also using (5.109) to eliminate q_1, we arrive at an expression for u_1 that only depends on y_T and u_1^*.

$$u_1 = u_1^*\frac{(y - y_i)}{(y_i - y_T)^2}\left[3y - 2y_T - y_i + 6y_T\frac{(y - y_T)}{(y_i - y_T)}\right]. \tag{5.114}$$

The same procedure can be used to solve the $\mathcal{O}(\delta^2)$ problem with the new boundary conditions $u_2(y_T) = u_2^*$. The solution is:

$$u_2 = u_2^*\frac{(y - y_i)}{(y_i - y_T)^2}\left[3y - 2y_T - y_i\right]. \tag{5.115}$$

Now we must find y_T to have a complete description of the solution. This is done by matching the shear stress to $\mathcal{O}(\delta)$ at y_T. This requires

$$u_y(y_T) \approx u_{0,y}(y_T) + \delta u_{1,y}(y_T) = 0. \tag{5.116}$$

Recall,

$$u_{0,y}(y_T) = -\frac{B}{y_y}(y_T - y_y) \sim \mathcal{O}(\delta). \tag{5.117}$$

Therefore, in order to have a balance of terms in (5.116) we need

$$u_{1,y}(y_T) = \frac{B}{y_y}\frac{(y_T - y_y)}{\delta}. \tag{5.118}$$

If we differentiate (5.114), we will then be able to use (5.118) to get an expression for y_T in terms of u_1^*.

$$u_{1,y} = \frac{u_1^*}{(y_i - y_T)^2}\left[3y - 2y_T - y_i + 3(y - y_i) + 6y_T\frac{2y - y_T - y_i}{y_i - y_T}\right]. \tag{5.119}$$

Which means,

$$u_{1,y}(y_T) = \frac{-2u_1^*}{(y_i - y_T)^2}\left(2y_i + y_T\right). \tag{5.120}$$

Combining (5.118) with (5.120) gives the following expression for y_T:

$$\frac{y_T - y_y}{\delta} = \frac{-2y_y u_1^*}{B(y_i - y_T)^2}(2y_i + y_T) \approx \frac{-2y_y u_1^*}{B(y_i - y_y)^2}(2y_i + y_y). \tag{5.121}$$

Note that this means y_T is given approximately by the same equation as the case $y_T < y_y$:

$$y_T \approx y_y - (2y_i + y_y)\left[\frac{u_p}{u_0^{pp}} - 1\right].$$

Now that y_T has been found, we know u_1 from (5.114) and u_2 from (5.115).

Note that the shear stress has not been matched at $\mathcal{O}(\delta^2)$ at the plug interface. This discontinuity is also present in the solution for the case $y_T < y_y$, but in that case it occurred at y_y, where the transition layer meets the outer solution. As a result, δ and h must be quite small (no more than about .08) for the solution to keep a smooth appearance.

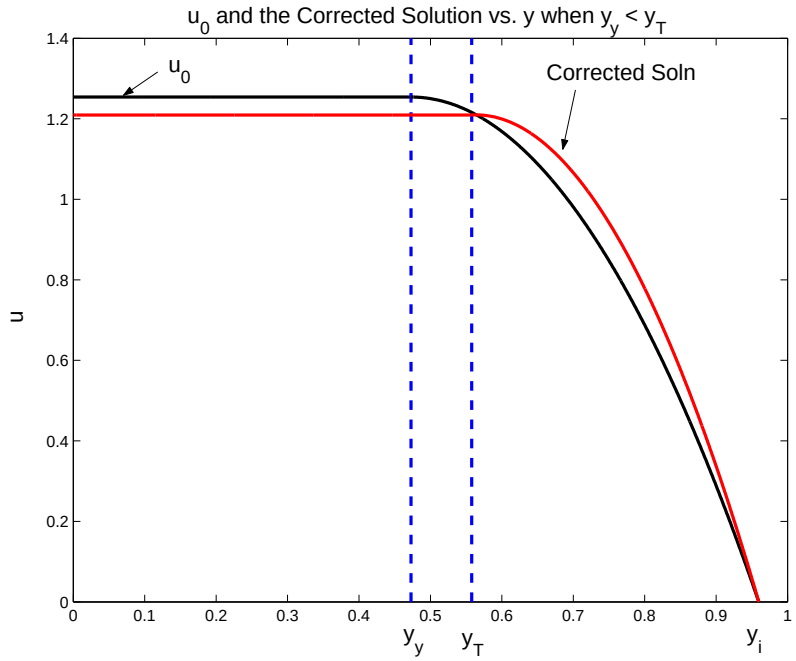

Figure 5.6: A plot of u_0 and u corrected to $\mathcal{O}(\delta^2)$ on a cross-section of the channel half-width where $y_T > y_y$. The parameters used were $B = 5$, $h = .05$, $\delta = .075$. The plug speed was determined by the method presented in §5.8.

5.6.1 Composite Solution for $y_T > y_y$

The complete description of the solution for $y_T > y_y$ is:

$$\begin{aligned} y > y_T \quad u \approx \quad & u_0^o + \delta u_1^o + \delta^2 u_2^o, \\ y \in [0, y_T] \quad u = \quad & u_p, \end{aligned}$$

where

$$y_T = y_y - (y_y + 2y_i)\left[\frac{u_p}{u_0^{pp}} - 1\right], \tag{5.122}$$

$$u_0^o = \frac{B}{2y_y}\left[(y_i - y_y)^2 - (y - y_y)^2\right], \tag{5.123}$$

$$u_1^o = u_1^* \frac{(y - y_i)}{(y_i - y_T)^2}\left[3y - 2y_T - y_i + 6y_T \frac{(y - y_T)}{(y_i - y_T)}\right], \tag{5.124}$$

$$u_2^o = u_2^* \frac{(y - y_i)}{(y_i - y_T)^2}\left[3y - 2y_T - y_i\right], \tag{5.125}$$

$$u_1^* = \frac{u_p - u_0^{pp}}{\delta}, \tag{5.126}$$

$$u_2^* = \frac{u_0^{pp} - u_0(y_T)}{\delta^2}, \tag{5.127}$$

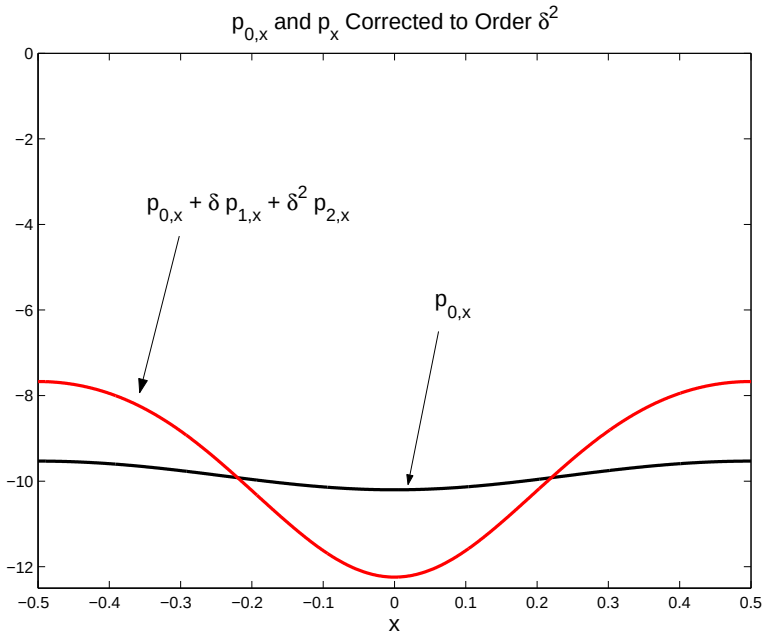

Figure 5.7: A plot of $p_{0,x}$ and the corrected pressure gradient for $B = 5$ and $h = .05$. The plug speed was determined by the method presented in §5.8. The value of δ does not affect this plot.

and

$$p_x = -\frac{B}{y_y} + \delta \frac{6u_1^*}{(y_i - y_T)^2}\left(\frac{2y_T}{(y_i - y_T)} + 1\right) + \delta^2 \frac{6u_2^*}{(y_i - y_T)^2} + \mathcal{O}(\delta^3). \tag{5.128}$$

5.7 Corrected Pressure Gradient

To get the corrected pressure gradient, (5.100) must be used for regions where $y_T < y_y$ and (5.128) must be used for regions where $y_T > y_y$. Fig. (5.7) shows a plot of $p_{0,x}$ and also p_x corrected to $\mathcal{O}(\delta^2)$. Notice that the correction terms give p_x a significantly greater amount of variation in x than is seen in $p_{0,x}$.

It is worth noting that the value of δ does not directly affect p_x, but the amplitude of the wall variation, h, does. This is because of $p_{1,x}$ having a factor of u_1^* and $p_{2,x}$ having a factor of u_2^*. For illustration, assume we are in a region where $y_T > y_y$, then if we were to use the definitions of u_1^* and u_2^* in (5.128) we would get,

$$p_x = -\frac{B}{y_y} + \frac{6\left[u_p - u_0^{pp}\right]}{(y_i - y_T)^2}\left(\frac{2y_T}{(y_i - y_T)} + 1\right) + \frac{6\left[u_0^{pp} - u_0(y_T)\right]}{(y_i - y_T)^2} + \mathcal{O}(\delta^3). \tag{5.129}$$

A similar thing happens in regions where $y_T < y_y$.

5.8 Plug Speed Determination

5.8.1 Derivation of Method to Determine the Plug Speed

Now, we devise a method to determine the plug velocity. Once the plug speed is determined, we will have a totally complete solution for the flow when the plug is intact.

We assume that there exists an intact plug for the calculations in this section. We will see in Chapter 6 that this assumption is not true if h is too large.

First, we refer to [7]. In §6, Prager develops the following minimum principle for stress of a slow visco-plastic flow. He states:

If $\mathbf{u}$ *is the solution velocity field, then the solution stress field minimizes the following functional:*

$$\mathcal{K}(p,\tau_{ij}) \equiv \frac{1}{4}\int_{\Omega}[|\tau - B| + \tau - B]^2 \, d\mathbf{x} \quad - \quad 2\int_{\partial\Omega}\sigma_{ij}u_i n_j \, ds. \tag{5.130}$$

Summation is implicit in the functional above with $u_1 = u$ and $u_2 = v$. Different plug speeds give different stress fields, which means we should choose u_p so that it minimizes $\mathcal{K}$.

Using the fact that $u_2 = 0$ throughout all of $\partial\Omega$ lets us write the second term as follows,

$$-2\int_{\partial\Omega}\sigma_{ij}u_i n_j \, ds = -2\int_{\partial\Omega}\langle u(-p+\tau_{xx}) \, , \; u\tau_{xy}\rangle \cdot \mathbf{n} \, ds.$$

Many more terms fall out when the rest of the boundary conditions are applied to u and τ_{ij} leaving,

$$-2\int_{\partial\Omega}\langle u(-p+\tau_{xx}) \, , \; u\tau_{xy}\rangle \cdot \mathbf{n} \, ds = 2\int_0^{y_i}[u\,p]_{x=\frac{1}{2}} \, dy - 2\int_0^{y_i}[u\,p]_{x=-\frac{1}{2}} \, dy.$$

However, we have shown that $p_y \sim \mathcal{O}(\delta^3)$, so if we keep only the $\mathcal{O}(\delta^2)$ terms and larger, then we can pull the pressure out of the integral to get

$$2p\,(1/2)\int_0^{y_i} u(1/2,y)\,dy - 2p\,(-1/2)\int_0^{y_i} u(-1/2,y)\,dy.$$

But we also know:

$$\int_0^{y_i} u(-1/2,y)\,dy = \int_0^{y_i} u(1/2,y)\,dy = 1.$$

That means the entire boundary integral reduces to

$$2[p(1/2) - p(-1/2)] = 2\int_{-1/2}^{1/2} p_x \, dx = 2\int_{-1/2}^{1/2} p_{0,x} + \delta p_{1,x} + \delta^2 p_{2,x} + \mathcal{O}(\delta^3) \, dx. \tag{5.131}$$

Note that the $\mathcal{O}(1)$ term does not depend on the choice of u_p, so it does not need to be considered in the final functional.

Now focus on the integral over the interior domain. We have different solution forms depending on whether $u_p < u^{pp}(x)$ or $u_p > u^{pp}(x)$. Furthermore, the flow is non-inertial, and we have taken $y_i(x) = 1 - h\cos(2\pi x)$, so our solution is symmetric about $x = 0$. Therefore, there must be some x_p such that:

$$\begin{aligned} u_p &> u^{pp}(x) \ \text{ for } \ |x| > x_p, \\ u_p &= u^{pp}(x) \ \text{ for } \ |x| = x_p, \\ u_p &< u^{pp}(x) \ \text{ for } \ |x| < x_p. \end{aligned}$$

From this point forward, we will restrict our attention to positive values of x only. We can do this because our solution is even about $x = 0$. From our asymptotic solution, we have

$$\begin{aligned} &\int_0^{1/2}\int_0^{y_i} [|\tau - B| + \tau - B]^2 \, dy \, dx = \\ &\quad \left\{ \int_0^{x_p}\int_{y_T}^{y_i} [|\tau^o - B| + \tau^o - B]^2 \, dy \, dx \right. \\ &\quad \left. + \int_{x_p}^{1/2} \left[\int_{y_T}^{y_y} [|\tau^i - B| + \tau^i - B]^2 \, dy \ + \ \int_{y_y}^{y_i} [|\tau^o - B| + \tau^o - B]^2 \, dy \right] \, dx \right\}. \end{aligned} \tag{5.132}$$

Let us first assume that we are in a region where $x > x_p$ which means $y_T < y_y$. Recall that in the inner region

$$\tau^i_{xy} = -B + \delta u_{2,\xi} + \mathcal{O}(\delta^2),$$

and

$$\tau^i = |\tau^i_{xy}| + \mathcal{O}(\delta^2) = B - \delta u_{2,\xi} + \mathcal{O}(\delta^2).$$

Therefore

$$\int_{y_T}^{y_y} [|\tau^i - B| + \tau^i - B]^2 \, dy = \int_{y_T}^{y_y} 4\delta^2 u^2_{2,\xi} + \mathcal{O}(\delta^3) \, dy.$$

Remember $u_{2,\xi}^2 = \frac{B^2\xi^2}{y_y^2}$ and $\xi = \frac{y-y_T}{\delta}$. Using this information, we get an expression in terms of y_y and y_T:

$$\int_{y_T}^{y_y} [|\tau^i - B| + \tau^i - B]^2 \, dy \approx \frac{4B^2}{y_y^2} \int_{y_T}^{y_y} (y - y_T)^2 \, dy = 4B^2 \frac{(y_y - y_T)^3}{3y_y^2} \sim \mathcal{O}(\delta^3).$$

For the integral in the fully yielded outer region, we know $\tau_{xx} \sim \mathcal{O}(\delta)$ because $h \sim \mathcal{O}(\delta)$. This means

$$\tau = |\tau_{xy}| + \mathcal{O}(\delta^4) = |\tau_{xy,0}| + \delta\tau_{xy,1} \text{ sign}(\tau_{xy,0}) + \delta^2\tau_{xy,2} \text{ sign}(\tau_{xy,0}) + \mathcal{O}(\delta^3).$$

Note that $\text{sign}(\tau_{xy,0}) = -1$. Therefore

$$\begin{aligned}
&\frac{1}{4}\int_{y_y}^{y_i} [|\tau - B| + \tau - B]^2 \, dy \\
&\quad = \int_{y_y}^{y_i} \left[|\tau_{xy,0}| - \delta\tau_{xy,1} - \delta^2\tau_{xy,2} - B + \mathcal{O}(\delta^3)\right]^2 \, dy \\
&\quad = \int_{y_y}^{y_i} \big\{(|\tau_{xy,0}| - B)^2 - 2\delta\tau_{xy,1}(|\tau_{xy,0}| - B) \\
&\qquad\qquad + \delta^2\left[\tau_{xy,1}^2 - 2\tau_{xy,2}(|\tau_{xy,0}| - B)\right] + \mathcal{O}(\delta^3)\big\} \, dy.
\end{aligned} \tag{5.133}$$

Note that the $\mathcal{O}(1)$ term in (5.133) above does not depend on u_p. For this reason, it can be neglected in the final functional we are considering. Dropping the $\mathcal{O}(1)$ term and writing the shear stresses in terms of the pressure gradients, the RHS of (5.133) becomes

$$\int_{y_y}^{y_i} -2\delta p_{1,x}|p_{0,x}|y(y - y_y) + \delta^2\left[p_{1,x}^2 y^2 - 2p_{2,x}|p_{0,x}|y(y - y_y)\right] + \mathcal{O}(\delta^3) \, dy. \tag{5.134}$$

Now, if we were in a region where $y_T > y_y$, the integral would have a lower limit of y_T instead of y_y. However, we shall see that this only makes a $\mathcal{O}(\delta^3)$ difference to (5.134). You can see this by noting that,

$$\begin{aligned}
&\int_{y_T}^{y_i} -2\delta p_{1,x}|p_{0,x}|y(y - y_y) + \delta^2\left[p_{1,x}^2 y^2 - 2p_{2,x}|p_{0,x}|y(y - y_y)\right] + \mathcal{O}(\delta^3) \, dy \\
&= \left\{\int_{y_y}^{y_i} -2\delta p_{1,x}|p_{0,x}|y(y - y_y) + \delta^2\left[p_{1,x}^2 y^2 - 2p_{2,x}|p_{0,x}|y(y - y_y)\right] + \mathcal{O}(\delta^3) \, dy\right. \\
&\left. - \int_{y_y}^{y_T} -2\delta p_{1,x}|p_{0,x}|y(y - y_y) + \delta^2\left[p_{1,x}^2 y^2 - 2p_{2,x}|p_{0,x}|y(y - y_y)\right] + \mathcal{O}(\delta^3) \, dy\right\};
\end{aligned}$$

and, the integral from y_y to y_T above is $\mathcal{O}(\delta^3)$ because the interval of integration is $\mathcal{O}(\delta)$ and the term $(y - y_y)$ is $\mathcal{O}(\delta)$ on this interval. Therefore, the expression in (5.134) is an accurate approximation for all x. However, the definitions of $p_{1,x}$ and $p_{2,x}$ vary depending on whether $x < x_p$ or $x > x_p$.

Now, by doing the integration and expanding the result it can be shown that,

$$|p_{0,x}| \int_{y_y}^{y_i} y(y - y_y)\, dy = \int_0^{y_i} u_0\, dy = 1. \tag{5.135}$$

This means that (5.134) can be written as

$$\int_{y_y}^{y_i} -2\delta p_{1,x} + \delta^2 \left[p_{1,x}^2 y^2 - 2p_{2,x}\right] + \mathcal{O}(\delta^3)\, dy. \tag{5.136}$$

When we include the boundary integral given by (5.131), the $\mathcal{O}(\delta)$ terms cancel and the resulting functional dependent on u_p to be minimized is

$$\mathcal{K}(u_p) = \int_0^{1/2} \int_{y_y}^{y_i} p_{1,x}^2 y^2 + \mathcal{O}(\delta^3)\, dy\, dx.$$

The integration in y can be done exactly. The higher order terms are then dropped, giving the final form of the functional,

$$\mathcal{K}(u_p) \approx \int_0^{1/2} \frac{p_{1,x}^2}{3} \left(y_i^3 - y_y^3\right)\, dx. \tag{5.137}$$

5.8.2 Results of Plug Speed Determination Method

A plot of $\mathcal{K}(x_p)$ is shown in Fig. 5.8. There is a clear minimum at $x \approx .2165$. Fig. 5.9 shows the relationship between h and x_p. One plot has $B = 5$ and the other has $B = 20$. Two things are evident from these plots. The first is that a higher Bingham number results in x_p being closer to the symmetry line $x = 0$. The other is that $x_p < .25$ for $h > 0$. This has been validated for very small values of both B and h that are not shown on in Fig. 5.9. For any Bingham number, as $h \longrightarrow 0$, we have $x_p \longrightarrow .25$.

Another interesting feature of the functional given in (5.8) is that it is independent of δ. However, we shall see in Chapter 6 that the existence of an intact plug is highly dependent on δ.

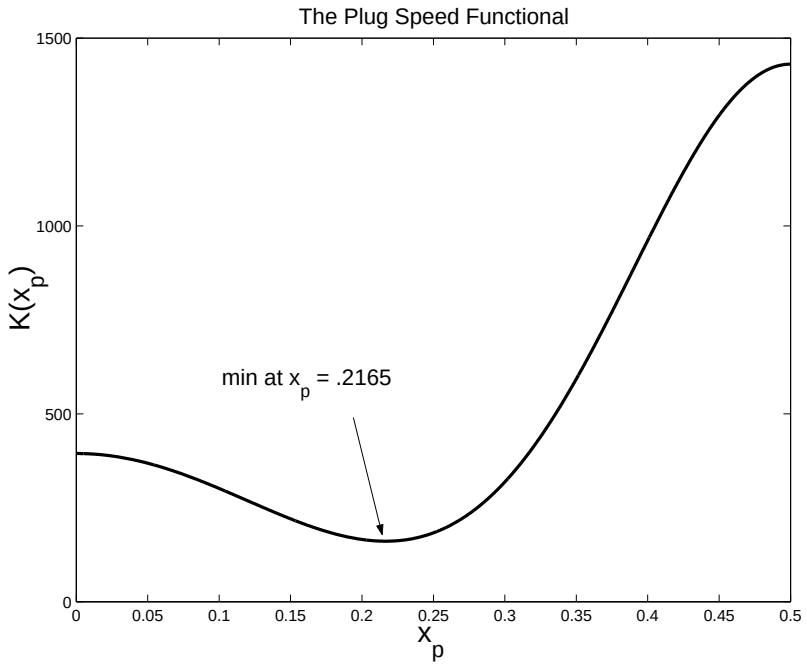

Figure 5.8: A plot of the plug speed functional using $B = 5$, $h = .02$, $\delta = .05$.

This means that δ strongly affects whether or not (5.8) is valid, but does not affect the value that (5.8) chooses for u_p. This comes from the fact that $p_{0,x}, p_{1,x}$ and $p_{2,x}$ only depend on y_i, y_y, and u_p.

The values obtained form the numerical simulations of Chapter 4 are shown by diamond shaped markers in Fig. 5.9. We see that the values from the numerical results are higher than the values from the analytic method derived in this section. We see that in the numerical results, we still have $x_p < .25$ and the trend that x_p decreases as h increases. We also see that for all h shown, x_p is smaller for $B = 20$ than it is when $B = 5$.

The relative difference between the analytic and numerical method is about 10 percent for $B = 5$ and $h = .05$. The relative difference seems to be less when either B or h is decreased.

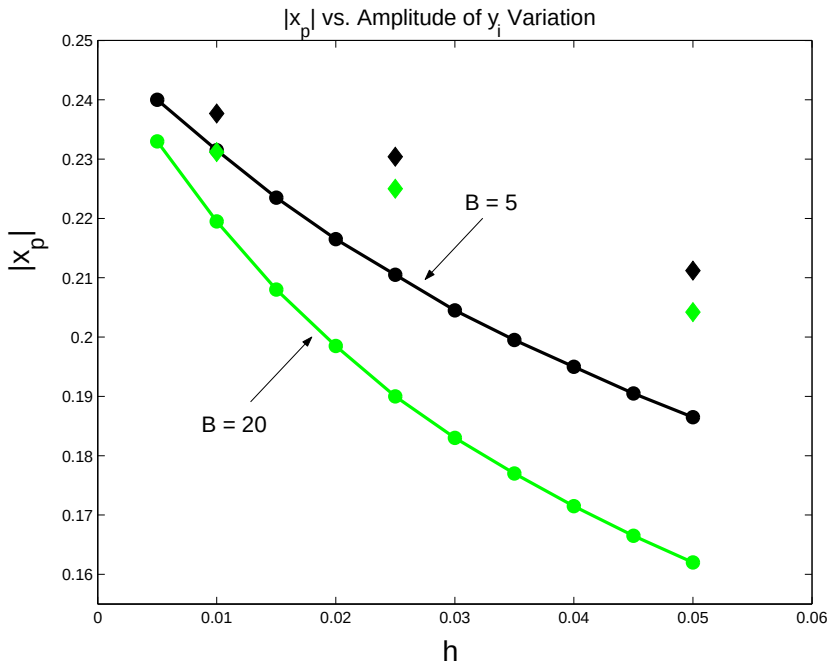

Figure 5.9: Plots of plug speeds for various amplitudes for $B = 5$ and $B = 20$. These plots are not affected by the value of δ. Some values determined from the numerical simulations of Chapter 4 are marked with diamonds of the appropriate color.

Chapter 6
Plug Breaking Criteria

6.1 A Solution for the Broken Plug

The term Pseudo-Plug Region characterizes a region in our domain where the stress on the centerline is slightly above the yield stress of the fluid. The result is a flow structure that resembles that of the plug region, but is actually yielded. We will not present the complete solution here because an inner layer is needed to match this solution to the fully yielded region, and a complete solution is not necessary to develop our plug breaking criteria. All that is needed is an expansion for the normal stress under the pseudo-plug flow structure.

To capture the behavior of the pseudo-plug region, we take expansions of the following form:

$$\begin{aligned} p &= p_0 + \delta p_1 + \delta^2 p_2 + \dots \ , \\ u &= u_0(y_i(x)) + \delta u_1(x,y) + \delta^2 u_2(x,y) + \dots \ , \\ v &= v_0 + \delta v_1 + \delta^2 v_2 + \dots \ . \end{aligned} \tag{6.1}$$

This means that $u_y \sim \mathcal{O}(\delta)$ in the pseudo-plug. The result of this expansion is a solution that is yielded at $\mathcal{O}(\delta)$ in both x and y (recall $y_i'(x) \sim h \sim \mathcal{O}(\delta)$).

Craster [2] used an expansion of this type to develop a solution for the flow of a visco-plastic fluid down an inclined plane.

Using the new expansions for velocity, we obtain new expansions for the strain components:

$$\begin{aligned} \dot{\gamma}_{xx} &= 2u_{0,x} + \delta 2u_{1,x} + \mathcal{O}(\delta^2), \\ \dot{\gamma}_{xy} &= \delta u_{1,y} + \delta^2(u_{2,y} + v_{0,x}) + \mathcal{O}(\delta^3). \end{aligned}$$

The second invariant of strain looks like

$$\dot{\gamma} = \delta \left(u_{1,y}^2 + 4u_{0,x}^2 + \delta[2u_{1,y}(u_{2,y} + v_{0,x}) + 8u_{0,x}u_{1,x}] + \mathcal{O}(\delta^2) \right)^{\frac{1}{2}} \sim \mathcal{O}(\delta). \tag{6.2}$$

For regions where $\tau > B$ the constitutive relations to leading order become

$$\tau_{xx} = \frac{B2u_{0,x}}{\delta(u_{1,y}^2 + 4u_{0,x}^2)^{\frac{1}{2}}} + \ldots \sim \mathcal{O}(\frac{1}{\delta}), \tag{6.3}$$

$$\tau_{xy} = \frac{Bu_{1,y}}{(u_{1,y}^2 + 4u_{0,x}^2)^{\frac{1}{2}}} + \ldots \sim \mathcal{O}(1). \tag{6.4}$$

The leading order equations are still

$$p_{0,y} = 0 \Longrightarrow p_0 = p_0(x),$$

$$p_{0,x} = \frac{\partial}{\partial y}(\tau_{xy,0}).$$

But now the expansion for τ_{xy} has changed, which when substituted gives

$$p_{0,x} = \frac{\partial}{\partial y}\left(\frac{Bu_{1,y}}{(u_{1,y}^2 + 4u_{0,x}^2)^{\frac{1}{2}}} \right). \tag{6.5}$$

We know p_0 is independent of y, so integrating both sides of (6.5) gives

$$yp_{0,x} = \frac{Bu_{1,y}}{(u_{1,y}^2 + 4u_{0,x}^2)^{\frac{1}{2}}}.$$

Finally, solving for $u_{1,y}$ we find

$$u_{1,y} = \pm \frac{2yp_{0,x}u_{0,x}}{(B^2 - p_{0,x}^2 y^2)^{\frac{1}{2}}}. \tag{6.6}$$

Equation (6.6) can be simplified if written in terms of $y_y = -\dfrac{B}{p_{0,x}}$:

$$u_{1,y} = \mp \frac{2yu_{0,x}}{y_y \sqrt{1 - \dfrac{y^2}{y_y^2}}}. \tag{6.7}$$

Because u_0 is also independent of y, we can integrate (6.6) in from y_y and have an explicit expression for u_1 depending on u_1^*:

$$u_1(x,y) = \pm 2u_{0,x}y_y \sqrt{1 - \frac{y^2}{y_y^2}} + u_1^* \quad \text{for} \quad y < y_y. \tag{6.8}$$

This is where we will leave the analysis. In order to complete the solution, we would have a matching layer at y_y that connects the pseudo-plug solution to the fully yielded outer solution.

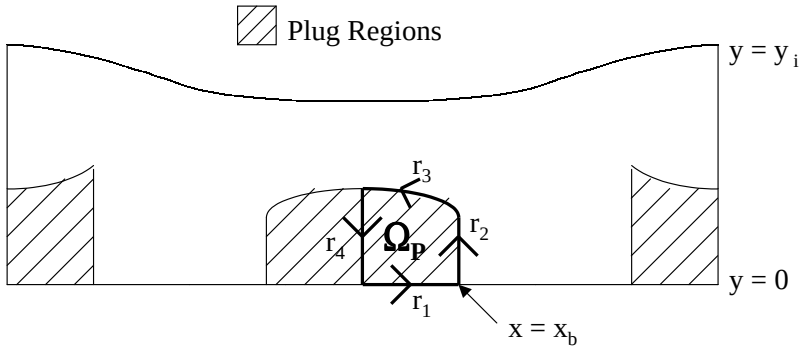

Figure 6.1: A sketch of the domain showing a broken plug. The integration uses a closed curve around the central plug region and is broken into four separate line integrals over r_1, r_2, r_3 and r_4.

6.2 Derivation of Plug Breaking Criteria

The general idea used to develop the criteria for when the plug breaks comes from Szabo and Hassager in their study of visco-plastic flows in eccentric annular geometries [8]. The idea is that when the plug is broken we could integrate the x-momentum equation around the central plug region and then use Green's Theorem to evaluate this integral. All of the terms can be directly evaluated except for the r_2 component of the line integral (see Fig. 6.1). The integrand for the r_2 component of the line integral involves τ_{xx}. When the plug is broken, we know that τ_{xx} changes orders compared to when the plug is not broken. Therefore, we can use the size of the other components of the line integral, r_1, r_3 and r_4, which balance with r_2 and which can be directly evaluated to determine the order of r_2 and hence whether or not the plug is broken. This is explained in more detail below.

First we integrate the x-momentum equation around the plug region (following the path $\mathbf{r} \equiv r_1 \bigcup r_2 \bigcup r_3 \bigcup r_4$, see Fig. 6.1). We then use the fact that $\tau_{xy} = 0$ on r_1.

$$\begin{aligned}
&\int_{\Omega_P} \nabla \cdot \langle -p + \delta^2 \tau_{xx} \, , \, \tau_{xy} \rangle \, d\mathbf{x} \\
&\quad = \oint_{\mathbf{r}} \langle -\tau_{xy} \, , \, -p + \delta^2 \tau_{xx} \rangle \, d\mathbf{r} \\
&\quad = \left\{ \int_{y_T(0)}^{0} -p \, dy + \int_{0}^{y_T(x_b)} -p + \delta^2 \tau_{xx} \, dy \right. \\
&\qquad \left. + \int_{x_b}^{0} -\tau_{xy}(x, y_T) + y_T' [-p(x, y_T) + \delta^2 \tau_{xx}(x, y_T)] \, dx \right\} = 0. \qquad (6.9)
\end{aligned}$$

Now, define

$$I(x_b) \equiv -\delta \int_0^{y_T(x_b)} \tau_{xx}(x_b, y)\ dy. \tag{6.10}$$

From (6.9) we have

$$\begin{aligned} \delta I(x_b) \quad = \quad & \left\{ \int_{y_T(0)}^{0} -p\ dy + \int_0^{y_T(x_b)} -p\ dy \right. \\ & \left. + \int_{x_b}^{0} -\tau_{xy}(x, y_T) + y_T'[-p(x, y_T) + \delta^2 \tau_{xx}(x, y_T)]\ dx \right\}. \end{aligned} \tag{6.11}$$

We will now use the force balance idea briefly discussed earlier to develop both necessary and sufficient conditions for the breaking of the plug.

The RHS of (6.11) will be evaluated up through $\mathcal{O}(\delta)$. $I(x_b)$ can be evaluated once we assume a form for $\tau_{xx}(x_b, y)$.

To develop the necessary condition for plug breaking, we assume that $\tau_{xx}(x_b, y)$ takes on the form given by the pseudo-plug solution, i.e. τ_{xx} is given by (6.3). Then, if there exists an $x_b \in [0, 1/2]$ satisfying (6.11), we say that the necessary condition is satisfied.

To develop the sufficient condition for plug breaking, we assume that $\tau_{xx}(x_b, y) = \dfrac{B}{\delta}$ along all of r_2. This will mean that $\tau(x_b, y) \geq B$ along all of r_2, and hence the plug must be broken. Then, if there exists an $x_b \in [0, 1/2]$ satisfying (6.11), we say that the sufficient condition is satisfied.

First we will simplify the RHS of (6.11). Ignoring terms of $\mathcal{O}(\delta^2)$ and higher, we see

$$\delta I(x_b) = [p_0 + \delta p_1]_{x=0} y_T(0) - [p_0 + \delta p_1]_{x=x_b} y_T(x_b) - B x_b + \int_0^{x_b} p_0(x) y_T'(x)\ dx. \tag{6.12}$$

Remember that the solution pressure field is unique only up to an arbitrary constant, $\bar{p}$. We have shown that at the maxima and minima of $y_i(x)$, that $p_y = 0$. So, we can choose $p = 0$ on the line $x = 0$ to set the arbitrary constant. We would then have $p_0 = p_1 = 0$ on the line $x = 0$. This means the first term on the RHS of (6.12) drops out. Integrating the last term by parts gives

$$\delta I(x_b) = -[p_0 + \delta p_1]_{x=x_b} y_T(x_b) - B x_b + [p_0 y_T]_0^{x_b} - \int_0^{x_b} p_{0,x} y_T\ dx. \tag{6.13}$$

Now we use the fact that $p_{0,x} = -\dfrac{B}{y_y}$ to get

$$\delta I(x_b) = -\delta p_1(x_b) y_T(x_b) + B \int_0^{x_b} \frac{y_T}{y_y} - 1 \; dx. \tag{6.14}$$

6.2.1 The Necessary Condition for Plug Breaking

To develop the necessary condition for plug breaking we use (6.3) to evaluate the RHS of (6.10). This gives

$$I(x_b) = B \int_0^{y_T(x_b)} \left(1 - \left[\frac{y}{y_y}\right]^2\right)^{\frac{1}{2}} dy \approx B \int_0^{y_y(x_b)} \left(1 - \left[\frac{y}{y_y}\right]^2\right)^{\frac{1}{2}} dy. \tag{6.15}$$

Using the substitution $\sin(\theta) = \frac{y}{y_y}$, the above equation becomes

$$I(x_b) \approx B y_y(x_b) \int_0^{\frac{\pi}{2}} \cos^2(\theta) d\theta = \frac{B y_y(x_b)}{2} \int_0^{\frac{\pi}{2}} 1 - \cos(2\theta) d\theta = \frac{B\pi y_y(x_b)}{4}. \tag{6.16}$$

With this methodology, we would satisfy the necessary condition for a broken plug when there exists an $x_b \in (0, 1/2)$ satisfying $F(x) = 0$, where

$$F(x) \equiv -\delta p_1(x) y_T(x) + B \int_0^{x} \frac{y_T}{y_y} - 1 \; dx - \delta \frac{B\pi y_y}{4}. \tag{6.17}$$

When there is no x_b that can satisfy this equation, the plug must remain intact.

6.2.2 Sufficient Condition for a Broken Plug

To develop the sufficient condition for a broken plug, we assume $\tau_{xx}(x_b, y) = B\delta$. With this assumption (6.10) becomes

$$I(x_b) = \int_0^{y_T(x_b)} B \; dy = B y_T(x_b). \tag{6.18}$$

This means that we would satisfy the sufficient condition for plug breaking when there exists an $x_b \in (0, 1/2)$ satisfying $G(x) = 0$, where

$$G(x) \equiv -\delta p_1(x) y_T(x) + B \int_0^{x} \frac{y_T}{y_y} - 1 \; dx - \delta B y_T. \tag{6.19}$$

When this condition is satisfied, we know that the plug should be broken.

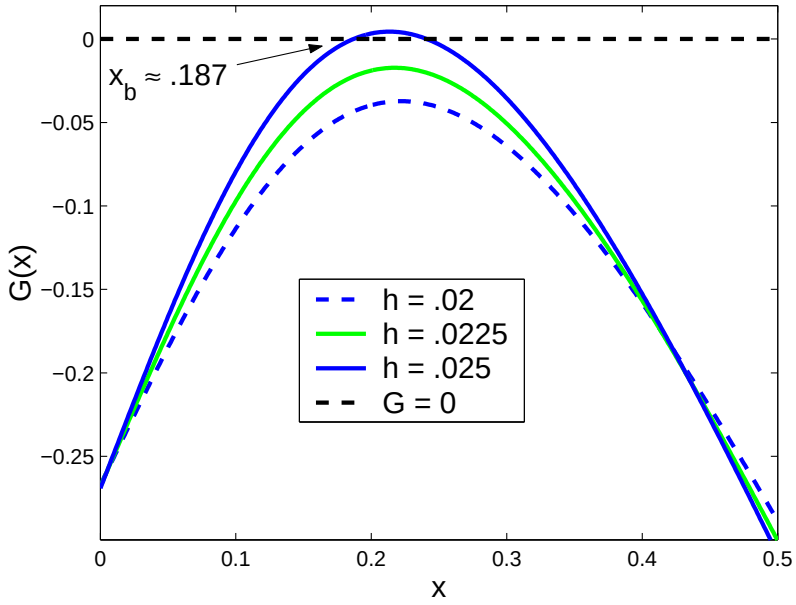

Figure 6.2: Plots of the sufficient breaking criteria with $B = 5$, $h \in [.02\ ,\ .025]$ and $\delta = .1$. The sufficient criteria is not satisfied for $h = .02$ or $.0225$, but it is satisfied for $h = .025$.

6.3 Discussion on Results of Breaking Criteria

Both $F(x)$ and $G(x)$ appear to always be concave down on $[0, 1/2]$ for any choice of parameters. We always have $F(0) < 0$ and $G(0) < 0$. As h increases, the apex of $F(x)$ and $G(x)$ increase. For any set of parameters there exists $h \in (0, 1)$ that will give an apex of both $F(x)$ and $G(x)$ greater than zero.

Figs. 6.2 and 6.3 each show $G(x)$ plotted for $h = .02, .0225$ and $.025$. In Fig. 6.2 we have a Bingham number of 5. We can see that the plug is not broken when $h = .0225$, but is broken when $h = .025$. Notice how in Fig. 6.3 we have increased the Bingham number to 20 and as a result the plug is not broken for $h = .025$. In fact, the apexes of all the curves have shifted down, away from the breaking line.

The trend of the Bingham number making the curves shift downward does not continue for large Bingham numbers. It seems that when B becomes large, it will cause p_x to break order which results in a poor approximation for u_p. The poor approximation for u_p then causes a poor approximation for y_T and the breaking criteria becomes inaccurate.

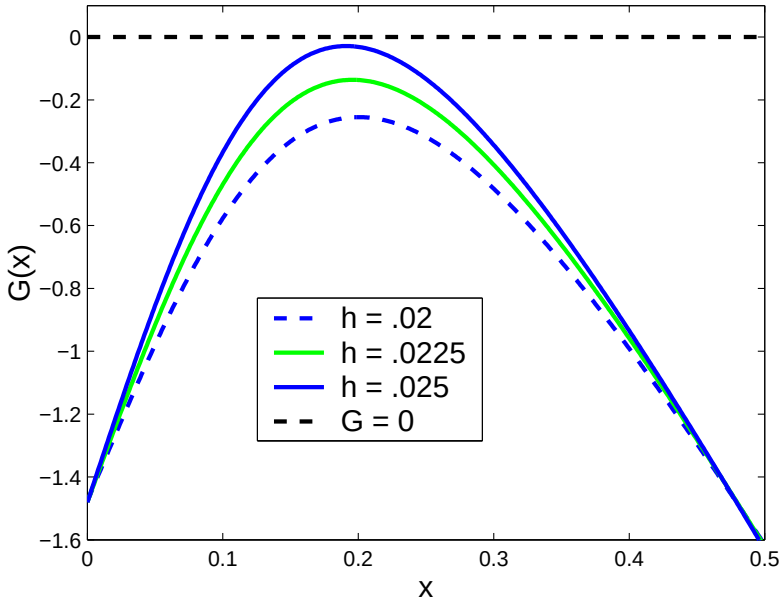

Figure 6.3: Plots of the sufficient breaking criteria with $B = 20$, $h \in [.02\ ,\ .025]$ and $\delta = .1$. The sufficient criteria is not satisfied for any $h \in [.02, .025]$.

The most dominant parameter in both the necessary and sufficient plug breaking conditions is δ. For example, the plots in Figs. 6.2 and 6.3 have $\delta = .1$. For $\delta = .1$, $B = 20$ the sufficient criteria for the plug breaking is satisfied at $h \approx .0235$. When $\delta = .25$ it requires $h \approx .091$ to satisfy the sufficient condition. The necessary condition with $\delta = .1$, $B = 20$ is satisfied for $h \approx .019$, but when we increase δ to .25 the necessary condition is now satisfied at $h \approx .065$.

When we compare the results of this section with our numerical simulations from Chapter 4, we find that the sufficient condition for plug breaking underestimates the amplitude required to break the plug in the numerical simulation.

For example, when using $B = 5$ and $L = 10$, the numerical simulations tell that the plug breaks for h somewhere between .04 and .05 (numerical results not shown). However, we can see from Fig. 6.2 that the sufficient condition for plug breaking is satisfied for some h between .0225 and .025. This trend of the sufficient condition of plug breaking being satisfied for a lower amplitude than the numerical results show a broken plug seems to hold for all parameter choices tried.

However, since the necessary condition for plug breaking yields an even smaller value than

the sufficient condition, we know that the necessary condition never overestimates the proper amplitude, so in this respect, we can trust it.

There is some agreement between the numerical simulations and the analytical results. Both approaches agree on the fact that a higher Bingham number requires a larger amplitude to break the plug (as long as B does not become very large). They also agree that a smaller δ requires a smaller amplitude to break the plug.

One observation that should be made is that when the amplitude is large enough to satisfy the sufficient condition for plug breaking, we see a change in appearance of the yield surface in the numerical simulations. For example, $\delta = .25, B = 5$ and $h = .085$ satisfies the sufficient condition for plug breaking. These are the parameters used in Fig. 4.2. When we look at this figure, we see that the yield surface near $x = -1/4$ (for x scaled) is curved in towards the centerline. However, $delta = .25, B = 5, h = .05$ are the parameters used in Fig. 4.5. These parameter choices does not satisfy the sufficient condition and we can see from the figure that there is no dip in the yield surface near $x = -1/4$ (for x scaled). This suggests that there is probably some transitional change in the flow structure between the "intact plug" solution and the "pseudo plug" solution (perhaps characterized by the size of $|y_y - y_T|$). This could account for the underestimation of the sufficient condition for plug breaking.

Chapter 7
Summary

Both numerical and analytical techniques are used to solve the unmodified Bingham model for slow flow in a long-thin gap of slowly varying width.

We have developed an analytical method to determine when an unbroken plug exists throughout the length of the gap as well as a complete description of the flow when the plug is intact. This flow description uses an asymptotic scheme based on the lubrication type scaling of the dimensional equations. This solution does not exhibit the classical inconsistencies that are usually present for a visco-plastic fluid scaled in this manner. The inconsistencies are resolved by assuming that there is an intact plug and constructing first and second order corrections to the flow that result in a fully rigid region. In order to attain the speed of this rigid solid a minimization principle for slow visco-plastic flow is used.

A method for numerical simulation based on finite elements is also presented, as well as results. This augmented Lagrangian method is ideal for a Bingham fluid because it permits the use of the full Bingham model and can compute the fully rigid regions.

Bibliography

[1] N.J. Balmforth and R.V. Craster. A consistent thin-layer theory for Bingham plastics. *J. Non-Newtonian Fluid Mech., 84*, 1999.

[2] N.J. Balmforth, R.V. Craster and R. Sassi. Shallow viscoplastic flow on an inclined plane. *J. Fluid Mech., 470,* 2002.

[3] G.K. Batchelor. *An Introduction to Fluid Dynamics*. Cambridge University Press, 1967.

[4] R. Glowinski. *Numerical Methods for Nonlinear Variational Problems*. Springer-Verlag, New York, 1984.

[5] C.C. Mei and M. Yuhi. Slow flow of a Bingham fluid in a shallow channel of finite width. *J. Fluid Mech., 431,* 2001.

[6] J.M. Piau. Flow of a yield stress fluid in a long domain: Application to flow on an inclined plane. *J. Rheol., 40(4),* 1996.

[7] W. Prager. On Slow Visco-Plastic Flow. Office of Naval Research Contract N7onr-35801. Taken from: *Studies in mathematics and mechanics, presented to Richard von Mises by friends, colleagues, and pupils.*, 1954.

[8] P. Szabo and O. Hassager. Flow of viscoplastic fluids in eccentric annular geometries. *J. Non-Newtonian Fluid Mech., 45(2)*, 1992.

[9] S.D.R. Wilson and A.J. Taylor. The channel entry problem for a yield stress fluid. *J. Non-Newtonian Fluid Mech., 65*, 1996.

[10] Th. Zisis and E. Mitsoulis. Viscoplastic flow around a cylinder kept between parallel plates. *Non-Newtonian Fluid Mech., 105*, 2002.